https://doi.org/10.5194/egusphere-2026-4579
Preprint. Discussion started: 7 September 2026

Variability in the Light Absorption Coefficients of phytoplankton, non-algal particles and colored dissolved organic matter in European Coastal Waters: A Two-Year Dataset in the Context of Historical Observations

Paola Potin[1], Isabella Mayot[1], Chiara Santinelli[2], Emmanuel Boss[3], Vittorio E. Brando[4], Margherita Costanzo[4,5], Victor Martinez-Vicente[6] and David Doxaran[1]

[1]Laboratoire d'Océanographie de Villefranche, UMR 7093, CNRS / Sorbonne Université, Villefranche-Sur-Mer, France
[2]Consiglio Nazionale delle Ricerche (CNR), Istituto di Biofisica (IBF), Pisa, Italy
[3]School of Marine Sciences, University of Maine, Orono, Maine
[4]Consiglio Nazionale delle Ricerche (CNR), Istituto di Scienze Marine (ISMAR), Rome, Italy
[5]Dipartimento Ingegneria civile, edile e ambientale, Università Sapienza, Rome, Italy
[6]Plymouth Marine Laboratory, UK

Correspondence to: Paola POTIN (paola.potin@imev-mer.fr)

Abstract. Coastal ecosystems play a major role in global biogeochemical cycles, which are challenging for ocean color satellite observations due to independent variability in the dynamics of phytoplankton, non-algal particles (NAP), and colored dissolved organic matter (CDOM). Field measurements and match-ups with satellite data are required to assess the validity of multi-sensor satellite products and optimize (or develop new) bio-optical inversion algorithms. For this purpose, the water reflectance, light absorption and backscattering properties of coastal waters must be measured together with the concentration, composition and size of the optically-active water constituents. In this study, we report the light absorption properties of phytoplankton, NAP and CDOM measured over two years along European coastal waters. Our results show distinct contributions of CDOM from the Atlantic to Mediterranean waters, with CDOM dominating the non-water absorption budget in most regions between 380 and 560 nm. Concerning phytoplankton absorption, the B95 model (Bricaud et al., 1995), linking chlorophyll concentration to phytoplankton absorption, reproduces the overall spectral shape but exhibits regional biases, with both over and underestimation, depending on the local phytoplankton community size structure, physiological photo-acclimation states, and specific taxonomic compositions. These results highlight limitations in the current parameterizations under contrasting coastal optical regimes. The mass-specific absorption coefficient of NAP (a_{NAP^*}) reflects variability in particle assemblages and river inputs, with a systematic significant contribution in the near-infrared (NIR) part of the spectrum. Overall, our results provide improved constraints on regional optical variability and contribute to the refinement of bio-optical models and ocean color algorithms in complex coastal environments.

https://doi.org/10.5194/egusphere-2026-4579
Preprint. Discussion started: 7 September 2026

1. Introduction

Coastal ecosystems are rich in marine biodiversity and play a major role in global biogeochemical cycles. They are among the most productive areas in the world despite their relatively small surface areas (less than 10 % of the global ocean) (Gattuso et al., 1998; Muller-Karger et al., 2005; Tran et al., 2019) and contribute disproportionately to carbon remineralization and storage. They are affected by strong anthropogenic pressures due to urbanization, tourism and agriculture. Indeed, a large proportion of the world population lives in coastal areas within 100 km from the sea (Feist and Levin, 2016; Atwood et al., 2024). Climate change exacerbates these pressures by inducing changes in temperature and coastal erosion and by altering fluvial inputs (freshwater but also suspended particulate matter (SPM), dissolved organic matter (DOM) and nutrients from draining basins) (Sale et al., 2014). These changes have direct consequences on biogeochemical processes notably related to the carbon cycle (Muller-Karger et al., 2005; Regnier et al., 2013; Ward et al., 2017; Keller et al., 2018).

In coastal waters, optically-active constituents such as non-algal particles (NAP), phytoplankton and Colored Dissolved Organic Matter (CDOM) vary independently unlike in open ocean waters. Throughout this study, the term Colored Dissolved Organic Matter (CDOM) is used for consistency, although Chromophoric Dissolved Organic Matter is also commonly used in the literature. These constituents can originate from various allochthonous sources, such as riverine input or sediment resuspension due to turbulent mixing, which may lead to a dominance of NAP and/or CDOM in total solar light absorption (Bowers et al., 2000). Phytoplankton particles, usually characterized by their Chlorophyll-a pigment (Chla, in mg m^{-3}) may however dominate the water light absorption properties particularly during the algal growing season as documented by Bricaud et al. (2004). This variability in the concentrations of the main optically-active water constituents affects the performance of bio-optical algorithms used to retrieve the concentrations of NAP, Chla and CDOM from the water-leaving reflectance signal, resulting notably in significant under- or over-estimation of Total Chlorophyll-a (TChla). Consequently, the calibration and validation of bio-optical algorithms and of derived satellite products in coastal waters require extensive concomitant in situ measurements of the biogeochemical, inherent and apparent optical (IOPs and AOPs) properties (Spyrakos et al., 2018).

Bricaud et al. (1995) determined the bio-optical relationships governing most offshore waters where optical properties are primarily driven by materials covarying with Chla. However, these relationships are often not applicable in coastal waters. Indeed, Babin et al. (2003a, b) highlighted that European coastal (Case-2) waters require specific regional parametrizations due to the uncoupled variability of Chla, NAP and CDOM, providing for the first comprehensive baseline for the IOPs for a wide diversity of coastal waters. Building on this work, Zibordi and Berthon (2024) compiled bio-optical measurements collected across European coastal waters between 1995 and 2022 and created the CoASTS-BiOMaP dataset. This dataset provides a long-term reference for contextualising observations and assessing their consistency with historical regional patterns. These parametrizations now require refinement relying on recent optical technologies in order to capture the variability induced by anthropogenic and climate-driven changes. Re-documenting the optical and biogeochemical properties of European coastal waters is required to assess the long-term spatio-temporal variability and potential environmental shifts.

https://doi.org/10.5194/egusphere-2026-4579
Preprint. Discussion started: 7 September 2026

In parallel, recent ocean color satellite sensors provide hyperspectral measurements in open ocean, coastal and inland waters, to potentially retrieve more information than multispectral sensors notably concerning phytoplankton species or functional groups (Bracher et al., 2017; Muller-Karger et al., 2018). Such recent satellite missions include the Plankton, Aerosol, Cloud, ocean Ecosystem (PACE) platform (Werdell et al., 2026) carrying the Ocean Color Instrument (OCI), a hyperspectral imaging radiometer designed for the observation of global ocean color, but also the EnMAP (Environmental Mapping and Analysis Program) (Guanter et al., 2015) and PRISMA (PRecursore IperSpettrale della Missione Applicativa) (Loizzo et al., 2018) which provide hyperspectral measurements over coastal and inland waters. Additionally, Pitarch and Brando (2025) developed an advanced synthetic hyperspectral dataset. Their theoretical models require high-quality in-situ validation to ensure they reflect the realistic variability of natural particles. Our study provides such a dataset.

The Traversing European Coastlines (TREC) expedition was conducted along the European coastal waters. The global objective was to better understand the interactions between land and sea. In this context, the Tara Europa and HyperBOOST projects were carried out aboard the Tara research vessel over two years (2023 and 2024). These projects respectively aimed to better understand marine biodiversity and the impacts of pollution and climate change on coastal ecosystems, by documenting the biogeochemical and hyperspectral optical properties of the diverse European coastal waters. An overview of the comprehensive dataset collected during the HyperBOOST project, including the different biological, biogeochemical, and optical measurements, is provided in the accompanying manuscript by Costanzo et al. (submitted) and in the associated dataset (Costanzo et al., 2026). The main aim of the present study is to better understand the absorption optical properties of European coastal waters in order to refine existing bio-optical inversion algorithms.

Here we report the concentrations and composition of the optically-active water constituents, namely SPM, Chla and DOM, and their respective relationships to hyperspectral light absorption coefficients considering 10 distinct bio-optical regions over the European coastal waters. Our results complement previous reference studies in this field including foundational studies (Babin et al., 2003b; Bricaud et al., 1995), historical in situ compilations (Zibordi and Berthon, 2024), and synthetic datasets developed for algorithm design (Pitarch and Brando, 2025). This study provides updated hyperspectral observations that enable the validation and refinement of new regional bio-optical parametrizations for ocean color inversion algorithms.

https://doi.org/10.5194/egusphere-2026-4579
Preprint. Discussion started: 7 September 2026

2. Data and Methods

2.1. Study area and sampling

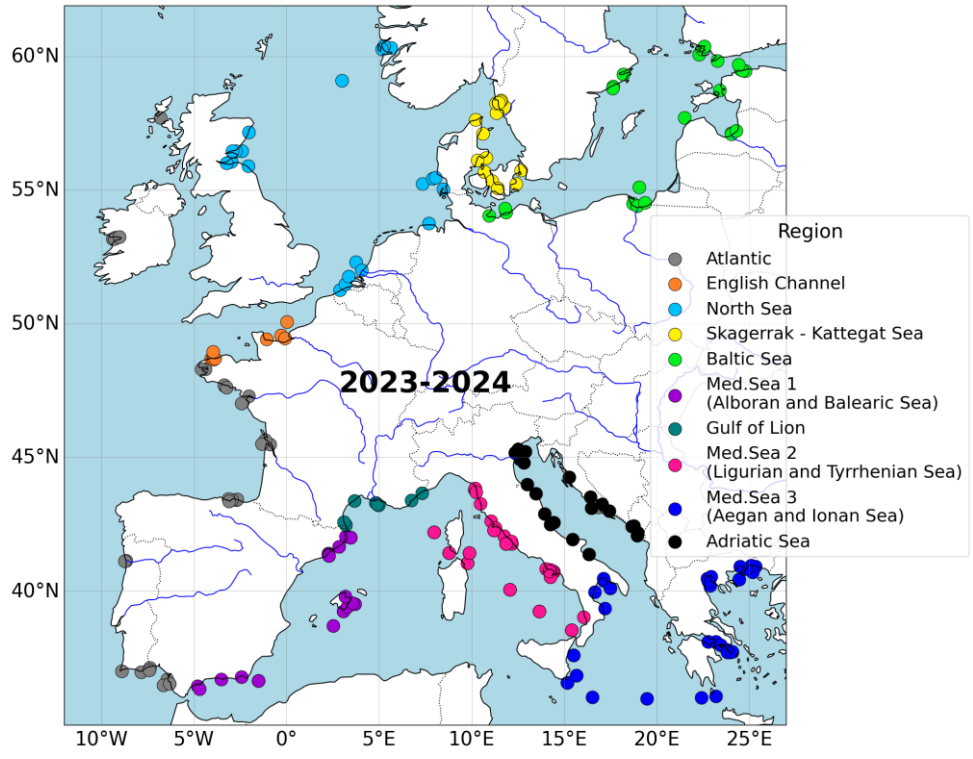

Figure 1: Map of the 202 field stations sampled during the Tara Europa cruise (April 2023–August 2024), colors refer to the 10 sub-basins.

Sampling was carried out along European Coastal waters for two consecutive years from April to September 2023 and from February to August 2024 aboard the Tara research vessel in the framework of the European Space Agency (ESA) HyperBOOST "Hyperspectral Bio-Optical Observations Sailing on Tara" project, which supported our participation in the Tara Europa expedition, which is part of the larger TREC research program. The HyperBOOST project not only aimed to measure the biogeochemical and optical properties of the wide diversity of European coastal waters in order to calibrate bio-optical algorithms. It also aimed to increase the number of matchups between field measurements and multi-sensor satellite observations for the validation of satellite products.

To maintain consistency with the TREC land–sea observational framework, marine sampling sites were selected in the vicinity of the coastal stations surveyed by the terrestrial sampling. Most stations were located approximately 1 km offshore in waters about 15 m deep, providing representative measurements of nearshore coastal waters.

Station locations were initially selected using high-resolution Chla climatologies derived from multi-year regional satellite products, which provided information on the expected spatial distribution and variability of coastal waters (Brando et al.,

https://doi.org/10.5194/egusphere-2026-4579
Preprint. Discussion started: 7 September 2026

2024). When required, station locations were further refined onboard in response to changing oceanographic conditions using interactive Leaflet maps displaying near-real-time environmental data (Marchese et al., 2024).

A total of 202 stations were sampled: 99 stations were sampled from April to November 2023 from the Baltic Sea to the Atlantic Ocean; 103 stations were sampled from February to August 2024 in the Mediterranean Sea (Med. Sea), including 14 offshore stations (Fig. 1).

10 sub-basins were identified, based on geographical boundaries of regional seas; due to the large number of regions in the Med. Sea stations were also grouped according to their light absorption properties (Fig. 1). At each station, water samples were collected within surface waters (at depth of 0.5 m) using Niskin bottles and filtered immediately after collection to retain suspended particles on glass-fiber filters. For CDOM measurements, water was filtered directly from the Niskin bottles using a portable filtration device implemented at CNR-IBF and a 0.2 µm Sterivex filter (SVGV010RS), rinsed with 200 mL of MilliQ water.Glass-fiber filters were kept frozen until laboratory analyses at the Laboratoire d'Océanographie de Villefranche (LOV). Filtrates were kept at 4 °C and in the dark and analysed within two weeks at the Institute of Biophysics of the Italian National Research Council (CNR-IBF).

2.2. Biogeochemical measurements

2.2.1. Suspended particulate matter

Water samples were transferred to clean bottles and kept homogeneous to measure the water turbidity (T, in Formazin Nephelometric Unit (FNU), in triplicates) according to the protocol established by Dogliotti et al. (2015). Then following the protocol defined by Neukermans et al. (2012), the measured mean Turb value was used to determine the optimal volume of water sample to be filtered through pre-weighed Whatman GF/F filters (25 mm diameter; 0.7 µm nominal pore size). This optimal volume ensures enough matter is retained by the filter for precise measurement of the concentration of suspended particulate matter (SPM, in g m^{-3}), but not so much that the filter clogs. The conversion table established by Neukermans et al. (2012) for 47 mm diameter GF/F filters was here adapted to 25 mm diameter filters, taking into account the ratio of filter clearances, i.e., preconized optimal volumes were divided by a ratio of about 3.5.

The SPM concentration was determined by the gravimetric method. The same optimal volume of seawater (V_{filtered}, in m^3) was filtered on six GF/F filters, pre-combusted (1 h at 450 °C) and pre-weighed (mass M_1, in g) in dry atmosphere. To remove residual salts from the filters, all filters were rinsed with fresh water. Each filter was then dried during 24 h at 60 °C. A second weighing under dry atmosphere provided the mass of the dry filter and all retained particles (M_2, in g). The SPM concentration (in g m^{-3}) was then obtained as:

$$\text{SPM} = \frac{(M_2 - M_1)}{V_{\text{filtered}}} \quad (1)$$

https://doi.org/10.5194/egusphere-2026-4579
Preprint. Discussion started: 7 September 2026

For each water sample, the mean SPM value and associated standard deviation (assumed to be representative of the measurement uncertainty) were determined from the sextuplicates. Across all samples, the mean propagated standard deviation associated with SPM measurements was 0.29 g m^{-3}. The mean relative uncertainty, calculated at the station level and averaged across the dataset, was 13.9 %.

The organic and inorganic fractions of the total suspended particulate matter were obtained according to the IOCCG Protocol Series (2021). Three filters used for SPM determination were burned 4 hours at 450°C to remove the organic material and weighed again. This final mass, corresponding to the mass of inorganic particles (M_3, in g), allowed the determination of the particulate inorganic fraction (PIF, in %), then by difference of the organic fraction (POF, in %):

$$\mathrm{PIF} = \frac{M_3 - M_1}{M_2 - M_1} * 100 \quad (2)$$

$$\mathrm{POF} = 100 - \mathrm{PIF} \quad (3)$$

For each water sample, the mean PIF and POF values and associated standard deviations (assumed to be representative of the measurement uncertainties) were determined from the triplicates. The particulate inorganic matter (PIM, g m^{-3}) and particulate organic matter (POM, g m^{-3}) concentrations were then calculated by multiplying PIF and POF, respectively, by the total suspended particulate matter concentration (SPM, g m^{-3}). Across all samples, the mean propagated standard deviation associated with PIM and POM measurements were both 0.13 g m^{-3}. Owing to the lower average concentration of PIM compared to POM, the corresponding mean relative uncertainties, calculated at the station level and averaged across the dataset, were 26.1 % and 14.6 %, respectively.

2.2.2. Phytoplankton pigments

The SAPIGH platform, a French National Analytical Service dedicated to HPLC (High Performance Liquid Chromatography) measurements was in charge to identify and quantify phytoplankton pigments (chlorophylls and carotenoids) in collected water samples. Following the protocol defined by Ras et al. (2008), the exact same volumes of water samples as for SPM determination were filtered through 25 mm Whatman GF/F filters. Filters were placed in vials, immediately frozen in liquid nitrogen then stored at -20°C onboard and -80°C on land until laboratory analyses at LOV. The method used is a modified version of the one developed by Van Heukelem and Thomas (2001) as described by Ras et al. (2008). Up to thirty pigments were quantified, when present. Note that in the current study the TChla concentration was defined as the sum of chlorophyll-a (Chla), divinyl chlorophyll-a (DVChla) and chlorophyllide-a (Chld-a), while only chlorophyll-a was considered in Babin et al. (2003b).

https://doi.org/10.5194/egusphere-2026-4579
Preprint. Discussion started: 7 September 2026

Triplicate measurements of TChla were performed at 15 stations. The mean standard deviation associated with TChla measurements was 0.12 mg m^{-3}. The mean relative uncertainty, calculated at the station level and averaged over these 15 stations, was 4.7 %.

Three classes of phytoplankton are commonly defined according to size: microplankton (>20 µm), nanoplankton (2-20 µm) and picoplankton (<2 µm). These size classes can be estimated using seven diagnostic pigments (Vidussi et al., 2001): Fucoxantin (Fuco), peridinin (Perid), 19'-hexanoyloxyfucoxanthin (Hexfuco), 19'-butanoyloxyfucoxanthin (Butfuco), alloxanthin (Allo), monovinyl chlorophyll-b + divinyl chlorophyll-b (TChlb) and zeaxanthin (Zea).

While (Vidussi et al., 2001) first proposed a diagnostic pigment approach to estimate phytoplankton size classes, Uitz et al. (2006) refined this method by introducing pigment-specific weighting coefficients to estimate the contribution of different phytoplankton size fractions to TChla. Chase et al. (2020), using co-located measurements of phytoplankton size distribution, revised the formulation with additional weighting terms, resulting in new equations for the estimation of phytoplankton size fractions. Although the parameterization of Chase et al. (2020) was the only work constructed based on flow cytometric observations, both approaches were primarily developed from datasets dominated by open-ocean environments and likely did not capture the specificities of coastal waters. In this study, a new coastal parameterization was developed to estimate phytoplankton size fractions in European coastal waters. The parameterization of Chase et al. (2020) was nevertheless retained as a benchmark because it spans a broad range of TChla concentrations while providing an independently evaluated reference for comparison, despite its limited representation of coastal regions. The combined Tara Europa and COASTlOOC (Massicotte et al., 2023) datasets were used to derive and evaluate the new parametrization across a wide range of European coastal environments.

The diagnostic pigment approach requires the estimation of TChla from the weighted contribution of diagnostic pigments. However, using the weighting scheme proposed by Uitz et al. (2006), the regression between the sum of diagnostic pigments and measured TChla was weak. In order to obtain a new regression model, a multiple regression analysis was performed (Table 1). In addition, parameterizations were developed separately for the Atlantic and Mediterranean datasets, and the corresponding regression coefficients are provided in Table 1. A non-negative least squares (NNLS) regression was applied to ensure physically meaningful (positive) contributions of diagnostic pigments. The model was independently validated using the COASTlOOC dataset.

For each parameterization, the three phytoplankton size fractions (micro-, nano-, and picophytoplankton) were calculated from the seven diagnostic pigments following the equations proposed by Uitz et al. (2006) and Chase et al. (2020). The corresponding equations were not reproduced here since they are directly available in the original publications.

The performances of the three parameterizations were compared using the linear regressions shown in Fig. 2. The slopes of the regression lines are 0.65 for COASTlOOC and 0.59 for Tara Europa using the parametrizations of Uitz et al. (2006). Corresponding slopes of 1.05 and 0.94 are obtained using the parameterization of Chase et al. (2020) (Fig. 2b). The linear regression obtained using the new parameterization is shown in Fig.2c, with regression slopes of 0.87 for COASTlOOC and 0.84 for Tara Europa. Although these slopes deviate more from the 1:1 line than those obtained with the Chase et al. (2020)

https://doi.org/10.5194/egusphere-2026-4579
Preprint. Discussion started: 7 September 2026

parameterization, the new parameterization yields slightly higher coefficients of determination (R2), indicating a comparable linear relationship with the observations.. Moreover, the new parameterization shows similar mean absolute differences (MAD) and mean relative differences (MRD) compared with the Chase et al. (2020) parameterization. For the HyperBOOST, MAD and MRD are 0.42 mg m^{-3} and 19.3 % compared with 0.32 mg m^{-3} and 19.1 % respectively. Similar for the COASTlOOC dataset, MAD and MRD are 0.98 mg m^{-3} and 23.4 % compared with 0.70 mg m^{-3} and 21.8 % respectively. The corresponding regressions obtained using the parameterizations developed for the Atlantic Ocean and the Mediterranean Sea are presented in Fig. 2e and Fig. 2f, respectively, highlighting the performance of region-specific coefficients within their respective basins.

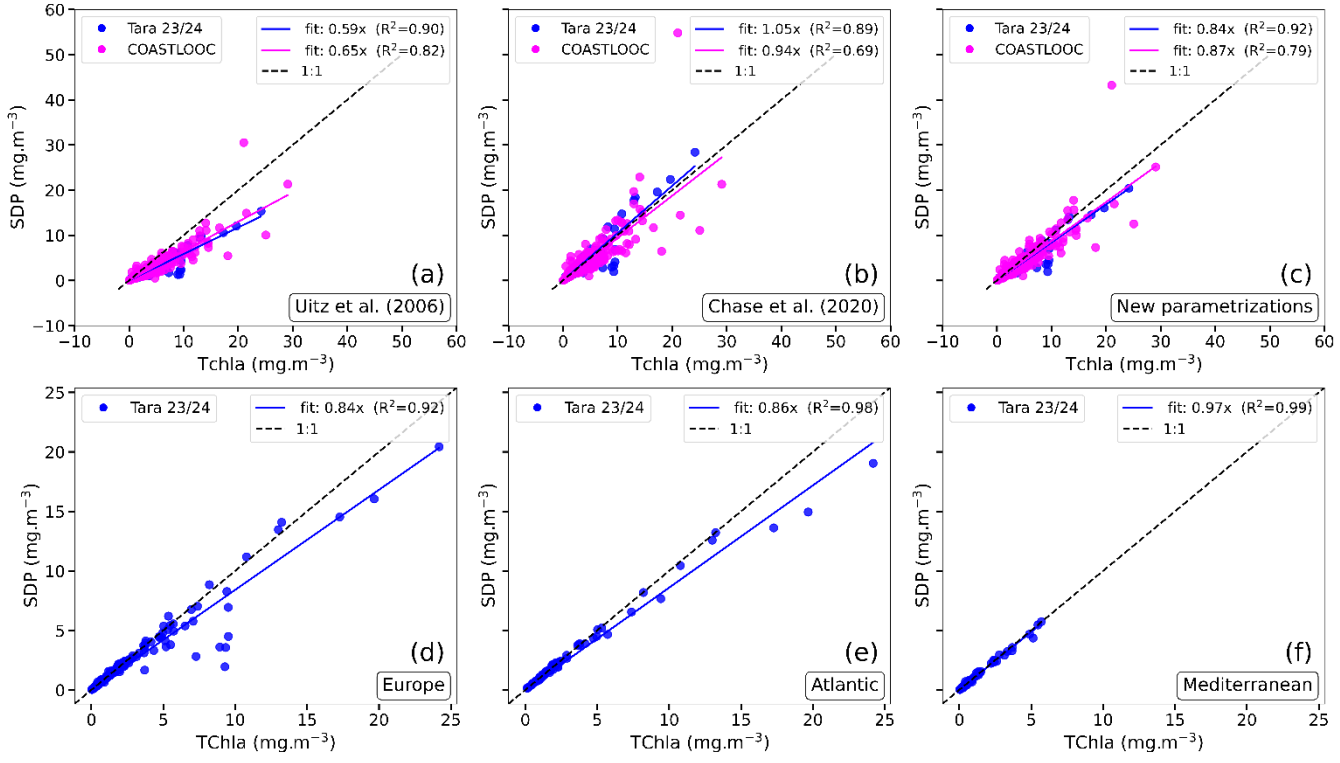

Figure 2: Comparison of linear regressions (a-f) between total chlorophyll a (TChla) and the sum of diagnostic pigments (SDP) obtained using the coefficients of Uitz et al. (2006), Chase et al. (2020) and the new parameterization considering the HyperBOOST and CoastlOOC datasets (top, from left to right). Linear regressions obtained using the new parametrization considering the whole Europe, Atlantic Ocean and Mediterranean Sea (bottom, from left to right).

Table 1. Values of pigment weights calculated in previous studies (Uitz et al. 2006 and Chase et al. 2020) and using the dataset from the present study.

	Literature		This study		
Pigment	Uitz et al. (2006)	Chase et al. (2020)	Europe	Atlantic	Mediterranean
Fucoxanthin	1.41	2.62	1.88	1.75	1.96

https://doi.org/10.5194/egusphere-2026-4579
Preprint. Discussion started: 7 September 2026

Peridinin	1.41	1.32	1.57	1.79	1.78
19'-Hexanoyloxyfucoxanthin	1.27	0.87	0.40	0.01	1.04
19'-Butanoyloxyfucoxanthin	0.35	0.00	2.12	3.14	0.01
Alloxanthin	0.60	2.64	3.76	3.37	3.08
Chlorophyll_b	1.01	0.94	1.40	1.71	2.12
Zeaxanthin	0.86	1.52	1.86	1.83	1.55

2.2.3. Particulate Organic Carbon

Particulate Organic Carbon (POC) concentrations were determined using 25 mm Whatman GF/F filters, the same GF/F filters used for SPM measurements (Doxaran et al., 2012; Blasco et al., 2021). Among the six replicate filters for SPM, three were used for POC analyses. Thus, filters underwent the same pre-treatment as for SPM analysis (pre-combusted at 450°C).

To accurately quantify the organic fraction, the particulate inorganic carbon (carbonates) was removed following a protocol optimized for mineral-rich waters (Blasco et al., 2021). Filters were acidified by adding 200 to 300 µL of 2 N HCl directly onto the filter and leaving them to react overnight. This liquid acidification step was selected to ensure complete decarbonation in samples rich in mineral matrices or resistant carbonates, which are common in coastal waters. Following acidification, samples were dried at 60 °C for at least 4 hours to remove residual water and excess acid. Carbon content was then measured by high-temperature combustion using Isotope Ratio Mass Spectrometry (IRMS), via an elemental analyzer coupled to a mass spectrometer. The isotopic data were normalized to the reference gas and corrected using certified standards.

All measurements were performed in triplicate, and final concentrations were corrected using blanks procedural filtrate blanks to account for both filter background and potential adsorption of dissolved organic carbon (DOC) onto the glass fiber matrix during filtration. The mean standard deviation associated with POC concentrations was 0.06 g m^{-3}. The average POC concentration was 0.29 ± 0.06 g m^{-3} (mean ± standard deviation), based on the variability among replicate measurements at each station.

2.2.4. Dissolved Organic Carbon

All the samples for dissolved organic carbon (DOC) were filtered directly from the Niskin bottles, using a portable filtration device implemented at CNR-IBF and a 0.2 um Sterivex filter (SVGV010RS), washed by 200 ml of MilliQ water. Samples for DOC were immediately acidified to pH < 2 by adding ultrapure 2M HCl. All the samples were immediately stored on board in the dark and at 4°C and analysed within 2 weeks from the sampling to minimise problems associated with the long storage.

https://doi.org/10.5194/egusphere-2026-4579
Preprint. Discussion started: 7 September 2026

DOC measurements were carried out with a Total Organic Carbon analyser (TOC-L, Shimadzu), by high temperature catalytic oxidation, following (Santinelli et al., 2015). Measurement quality was assessed twice daily by comparison of data with DOC Consensus Reference Waters (CRM) (Hansell, 2005) (batch #23/02, measured concentration: 41.4 ± 1.6 µM, n =55).

2.3. Optical measurements

2.3.1. Particle absorption

For particulate light absorption coefficient measurements, seawater was filtered on Whatman GF/F filters (25 mm), considering the same volumes as the ones filtered for SPM determination. Filters were then immediately frozen and stored in petri dishes at low temperatures (-20°C) onboardnear and during transport (in dry ice) up to laboratory analyses at LOV.

Light absorbance was measured using a Perkin Elmer Lambda 850 UV/Vis spectrophotometer equipped with an integrating sphere (150 mm), from 300 nm to 800 nm with an increment of 1 nm. The method used was the quantitative filter technique (integrating sphere (IS) mode) established by Röttgers and Gehnke (2012) detailed in the IOCCG Protocol Series (2018). Each filter was placed in the center of the integrating sphere perpendicular to the light beam, with particles facing it. The optical density (OD) was successively measured on blank filters (OD_{blank}), saturated with pure water, then on sample filters (OD_{sample}), at ambient temperature to compute the optical density of particles retained on filters as:

$$OD_{\mathrm{f}}(\lambda) = OD_{\mathrm{sample}}(\lambda) - OD_{\mathrm{blank}}(\lambda) \quad (4)$$

Where λ is the wavelength.

A second correction is then applied to account for the pathlength amplification of the filter pad technique:

$$OD_{\mathrm{s}}(\lambda) = 0.323 * OD_{\mathrm{f}}(\lambda)^{1.0867} \quad (5)$$

The particulate absorption coefficients (a_x, in m^{-1}) were finally computed as:

$$a_{\mathrm{x}}(\lambda) = \frac{\ln(10) * OD_{\mathrm{s}}(\lambda)}{V/A} \quad (6)$$

Where V is filtered volume (in m^3) and A is the effective area of the filter (m^2).

The first particle absorption coefficient measured was a_p, the total particulate absorption coefficient. Then each filter was placed for minimum 1 h and maximum 24 h on a filet holder with the funnel filled with methanol for depigmentation. The methanol and all dissolved phytoplankton pigments were flushed, the filter saturated with pure water placed again in the center

https://doi.org/10.5194/egusphere-2026-4579
Preprint. Discussion started: 7 September 2026

of the integrating sphere to measure the light absorption coefficient of non-algal particles: a_{NAP}. Finally, the light absorption coefficient of algal particles was determined as the difference:

$$a_{PHY}(\lambda) = a_p(\lambda) - a_{NAP}(\lambda) \quad (7)$$

Any residual significant a_{PHY} values obtained from 700 to 750 nm were assumed to be measurement errors, and the average a_{PHY} (700-750 nm) value was subtracted to the whole a_{PHY} spectrum (Babin et al., 2003b; Babin and Stramski, 2004).

The specific absorption coefficient of phytoplankton a_{PHY}^* (in m^2 (mg Chla)$^{-1}$) was calculated by dividing a_{PHY} by the TChla concentration. Results were compared with those predicted by the model of Bricaud et al. (1995):

$$a_{PHY}^*(\lambda) = A(\lambda) * \mathrm{TChla}^{-B(\lambda)} \quad (8)$$

Where A(λ) and B(λ) are tabulated spectral coefficients obtained from Table 2 of Bricaud et al. (1995)

For NAP, the mass-specific absorption coefficient (a_{NAP}^* (in $m^2 g^{-1}$) was obtained by dividing a_{NAP} by the SPM concentration. A nonlinear exponential model was fitted to a_{NAP} spectra to estimate the exponential spectral slope coefficient (S_{NAP}, in nm^{-1}) between 380 and 730 nm, excluding the 400-480 and 620-710 nm ranges to avoid any residual pigment absorption (Babin et al., 2003b). Only spectra passing the quality-control criteria were retained, resulting in 201 valid spectra. One spectrum was excluded due to low fitting performance (R^2 <0.95) (Estapa et al., 2012; Röttgers and Gehnke, 2012).

$$a_{NAP}(\lambda) = a_{NAP}(\lambda_r) * e^{-s_{NAP}(\lambda-\lambda_r)} + B \quad (9)$$

Where λ_r is the reference wavelength (here 443 nm) and B is an offset.

2.3.2. CDOM absorption

All the samples for CDOM were filtered directly from the Niskin bottles, using a portable filtration device implemented at CNR-IBF and a 0.2 µm Sterivex filter (SVGV010RS), washed by 200 ml of MilliQ water.

CDOM absorbance spectra were measured between 230 and 700 nm, with a resolution of 0.5 nm, using a UV–Vis spectrophotometer (UV-2600i, Shimadzu) with a 10 cm quartz cuvette. Three spectra were registered for each sample and the average was reported. The mean standard deviation associated with CDOM absorbance measurements at 443nm was 0.009 m^{-1}. The mean relative uncertainty, calculated at the station level and averaged across all samples, was 10.2 %. The absorbance spectra of ultrapure Milli-Q water, measured in the same conditions as the samples, was subtracted from each sample spectrum. Initial, intermediate and final blanks were measured to check for the cleanliness of the cuvette and the instrument functioning. The light absorption coefficient (m^{-1}) was calculated by following the equation:

https://doi.org/10.5194/egusphere-2026-4579
Preprint. Discussion started: 7 September 2026

$$a_{\mathrm{CDOM}}(\lambda) = 2.303 * \frac{A(\lambda)}{L} \quad (10)$$

where A(λ) is the absorbance at the wavelength λ and L is the cuvette pathlength expressed in m. An exponential model was fitted to a_{CDOM} to estimate the spectral slope between 350 and 500 nm ($S_{350\text{-}500}$) for comparison with the study of Babin et al. (2003b). Before fitting, a baseline correction was applied by subtracting the mean absorption coefficient between 680 and 690 nm from the entire spectrum. The exponential fits between 350 and 500 nm showed high agreement with the measured spectra ($R^2 > 0.94$ for all stations), and all spectra were therefore retained for subsequent analyses.

$$a_{\mathrm{CDOM}}(\lambda) = a_{\mathrm{CDOM}}(\lambda_r) * e^{-s_{\mathrm{CDOM}}(\lambda-\lambda_r)} \quad (11)$$

$S_{350\text{-}500}$ or S_{CDOM} (nm^{-1}) as defined by Babin et al. (2003b) describes the approximate exponential rate of decrease in absorption with increasing wavelength in this range. The mean standard deviation associated with $S_{350\text{-}500}$ estimates was 0.0007 nm^{-1}. The mean relative uncertainty, calculated at the station level and averaged across all samples, was 4.7 %.

In this study, the absorption budget was established using all absorption values from non-algal particles, CDOM and phytoplankton. For a_{CDOM}, the exponential model fitted over the 350–500 nm spectral range was used to reconstruct the absorption spectrum from 350 to 750 nm, and these modeled values were used in the absorption budget.

3. Results & Discussion

3.1. Variability of Absorption Components

The variability of the TChla, SPM, POC and POM components across all the studied regions spans at least three orders of magnitude, whereas the $a_{\mathrm{CDOM}}(443)$ and DOC spans only two orders of magnitude (Fig. 3). There is a general covariance among these six variables, indicating that the waters were not dominated by a single constituent. This means that when one component is high, the others are generally also relatively high. Some extreme values are also observed, particularly in estuaries, with SPM exceeding sometimes 100 g m^{-3}. There is also a strong linear relationship between SPM and turbidity. Overall, the distribution is consistent with the variability reported by Babin et al. (2003b).

The observed variability reflects the complexity of coastal waters, where the optical properties are controlled by the combined variability of phytoplankton biomass, suspended particles, and CDOM rather than by biomass alone. The relationship between POC and SPM is an indicator of particle composition. Samples above the linear regression indicate organic dominance whereas samples below it suggests a high mineral or sedimentary influence.

https://doi.org/10.5194/egusphere-2026-4579
Preprint. Discussion started: 7 September 2026

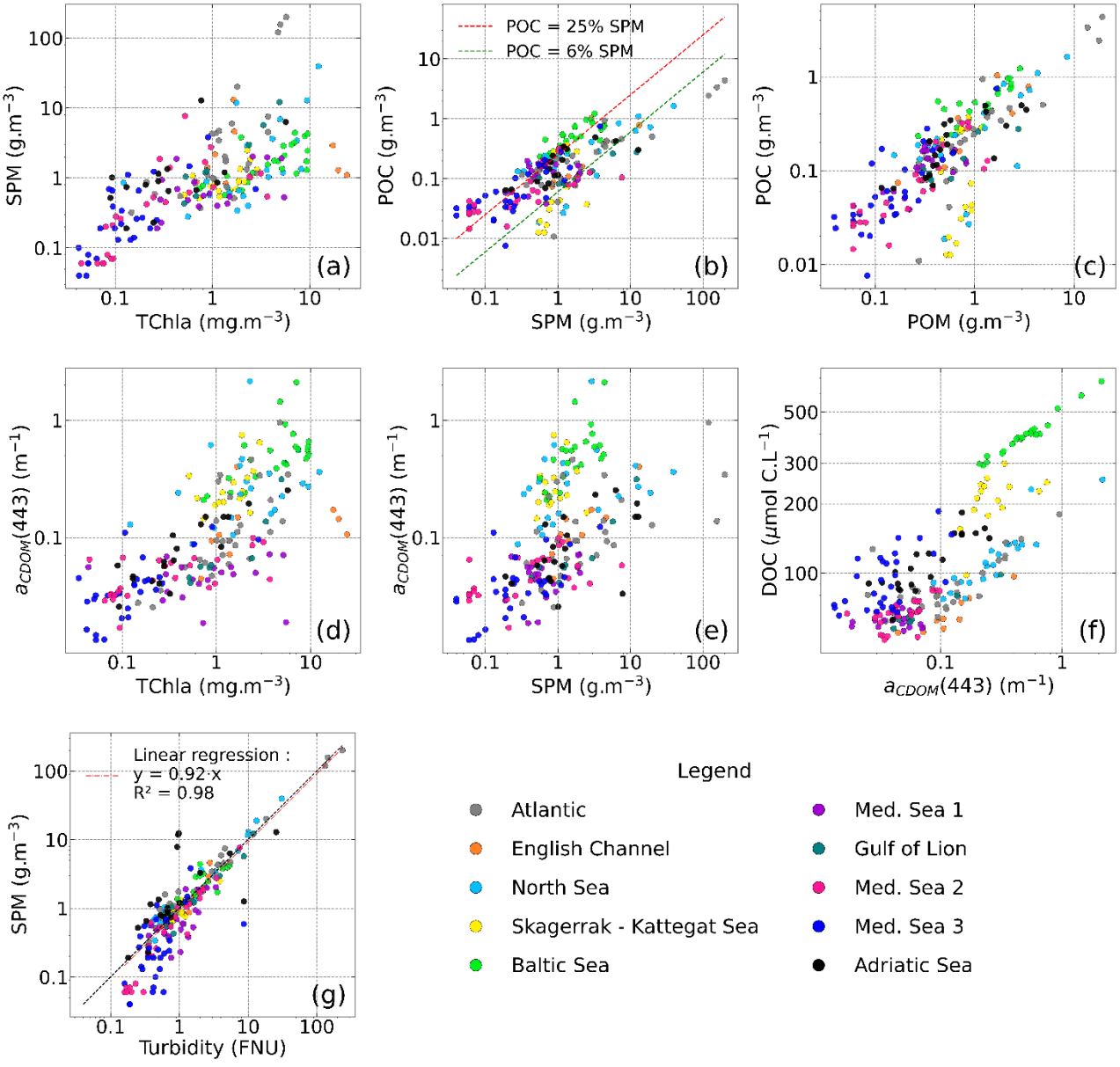

Figure 3: Scatterplots of (a) SPM versus TChla, (b) POC versus SPM (c) a_{CDOM}(443) versus TChla, (d)POC versus POM, (e) a_{CDOM}(443) versus SPM, (f) DOC versus a_{CDOM}(443), (g) SPM versus Turbidity for samples along European coastal waters by regions. Error bars are omitted for clarity due to the large number of observations. Analytical uncertainties associated with SPM, TChla, POC, and POM measurements are reported in the Data and Methods section.

3.2. CDOM absorption

In coastal waters, the contribution of CDOM to the total light absorption between 380 and 560 nm is usually dominant compared to that of phytoplankton or other particles (Babin et al., 2003b), it can be therefore used as a tracer of terrigenous inputs, allowing to get insights into the complex biogeochemical processes at the land-sea interface. In this section, the regional

https://doi.org/10.5194/egusphere-2026-4579
Preprint. Discussion started: 7 September 2026

variability of CDOM is examined across the 10 bio-optical regions to update historical baselines and capture potential environmental shifts.

The mean (non-modeled) CDOM absorption spectra between 350 and 700 nm show a high spatial variability across for the 10 studied regions (Fig. 4a). The highest values are observed in the Baltic Sea, the lowest ones in all the Med Sea sub-basins and intermediate values in the Atlantic regions. $S_{350\text{-}500}$ ranges from 0.010 to 0.026 nm^{-1} with a global mean value of 0.016 nm^{-1} (Fig. 4b) slightly lower than the global average reported by Babin et al. (2003b) (0.0176 nm^{-1}) in European coastal waters. This difference remains relatively small compared with the variability observed across the study area. The distribution exhibited two main groups: a first group, comprising all regions except the Baltic Sea and the Skagerrak–Kattegat Sea, with $S_{350–500}$ values between 0.010 and 0.018 nm^{-1}, and a second group, composed of the Baltic Sea and the Skagerrak–Kattegat Sea, with values between 0.018 and 0.020 nm^{-1}. A single extreme value (0.026 nm^{-1}) was observed at a return leg offshore station, where very low a_{CDOM} absorption was measured. This value should be interpreted with caution, as the weak CDOM absorption signal at this station reduces the robustness of the exponential fit used to estimate the spectral slope. Mean $S_{350\text{-}500}$ values ranged from 0.013 nm^{-1} in the Med Sea (Med Sea. 1 and 3) to 0.019 nm^{-1} in the Baltic Sea (Fig. 4c). Most European regions exhibited intermediate values, whereas the Baltic Sea and the Skagerrak–Kattegat displayed the highest mean spectral slopes and two Mediterranean regions displayed the lowest values (Fig. 4c). Table 2 also highlights marked regional variability in the $a_{CDOM}(443)$/DOC ratio. The highest ratios were observed in the North Sea (0.22 m^2 g C^{-1}), Atlantic Ocean and English Channel, followed by the Baltic Sea and the Skagerrak–Kattegat Sea. Intermediate values characterized the Gulf of Lion, whereas the Adriatic Sea and the three Mediterranean sub-basins consistently exhibited the lowest ratios (0.036–0.065)

The Baltic Sea is characterized by high CDOM absorption ($a_{CDOM}(443) = 0.56\ m^{-1}$), reflecting substantial inputs of terrestrially derived dissolved organic matter (Massicotte et al., 2023). The relatively high $S_{350–500}$ observed in this region is consistent with the distinctive spectral characteristics of terrestrially influenced DOM described by Helms et al. (2008). The good linear correlation between DOC and $a_{CDOM}(443)$ in this basin (Fig. 3f), suggests a common origin for both DOC and CDOM, consistent with observations from river-influenced coastal waters by Matsuoka et al. (2017).

Compared to the Baltic Sea, the lowest spectral slope $S_{350\text{-}500}$(<0.014 nm^{-1}) were observed in Med Sea 1 and Med Sea 3, whereas the other Mediterranean regions exhibited intermediate values. The presence of offshore stations in Med Sea 3 likely contributes to the low spectral slopes observed in this region. Our results agree with the decrease in $S_{350\text{-}400}$ values moving from freshwater to marine waters previously reported by Helms et al. (2008). $S_{350\text{-}500}$ values in the Med Sea 2 and the Gulf of Lion are lower than the range (0.018–0.026 nm^{-1}) reported by Para et al. (2010) for the same region. This difference could be explained by distinct oceanographic conditions. Para et al. (2010) associated their lowest spectral slope (0.014 nm^{-1}) with vertical mixing events that introduced older CDOM from deeper waters into the surface layer. Mediterranean regions also exhibit the lowest $a_{CDOM}(443)$/DOC ratio (Table 2) suggesting differences in DOM pool with a predominance of non-absorbing organic compounds in this basin.

https://doi.org/10.5194/egusphere-2026-4579
Preprint. Discussion started: 7 September 2026

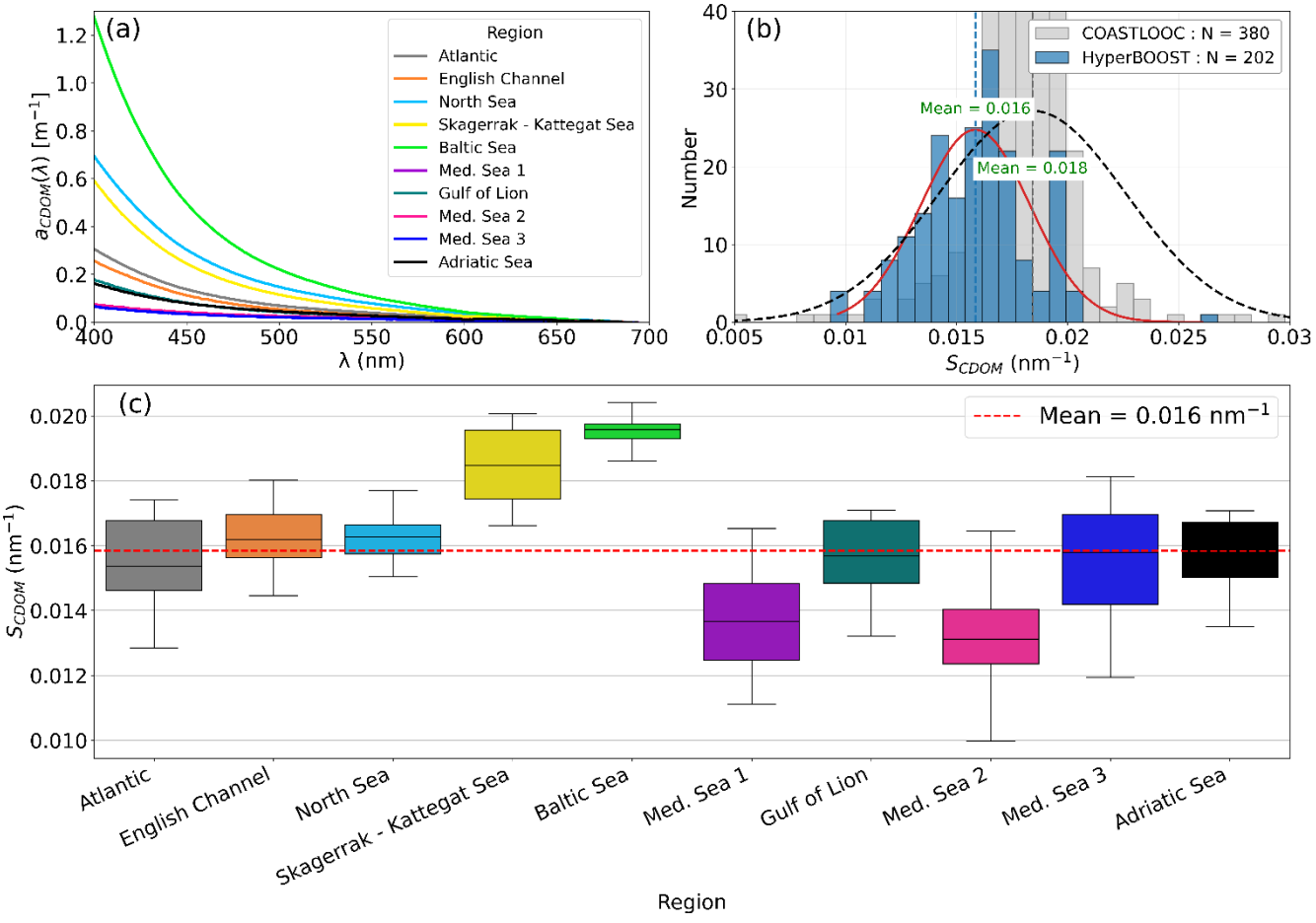

Figure 4: (a) Mean absorption spectra of CDOM for 10 studied regions. (b) Frequency distribution of the spectral slope $S_{350\text{-}500}$ (N = 202 stations) with Gaussian Curve shown as a red line. (c) Boxplot illustrating the regional variability of $S_{350\text{-}500}$ across the 10 study areas.

355 **Table 2: Summary statistics (mean ± SD, range) of $a_{CDOM}(443)$/DOC ratio in [m^2 (g C)$^{-1}$] by region.**

	$a_{CDOM}(443)$/DOC (m^2 g C^{-1})	
Region	Mean ± SD	Range
Atlantic (N = 29)	0.135 ± 0.091	0.018 – 0.442
English Channel (N = 9)	0.164 ± 0.078	0.067 – 0.345
North Sea (N = 22)	0.22 ± 0.128	0.08 – 0.703
Skagerrak – Kattegat Sea (N = 16)	0.116 ± 0.055	0.074 – 0.252
Baltic Sea (N = 23)	0.113 ± 0.046	0.059 – 0.259
Med. Sea 1 (N = 19)	0.063 ± 0.023	0.026 – 0.102
Gulf of Lion (N = 8)	0.104 ± 0.07	0.059 – 0.265

https://doi.org/10.5194/egusphere-2026-4579
Preprint. Discussion started: 7 September 2026

Med. Sea 2 (N = 25)	0.062 ± 0.02	0.021 – 0.102
Med. Sea 3 (N = 30)	0.036 ± 0.018	0.015 – 0.100
Adriatic Sea (N = 21)	0.065 ± 0.031	0.024 – 0.148

3.3. Phytoplankton Absorption

The mean phytoplankton-specific absorption spectra (a_{PHY}^*) across ten studied regions over the 400-700 nm spectral range are compared with the empirical power-law model established by the B95 (Fig. 5). The spectra derived from the B95 parameterization capture the overall spectral shape observed in most regions. However, the model significantly overestimates absorption in two Med sub-basins (Med Sea 2 and 3). In the Med Sea 2, at 443 nm, mean a_{PHY}^* measured values average are around 0.04 $m^2.mg^{-1}$ whereas the B95 model predicts values near 0.06 $m^2.mg^{-1}$. Overall, the mean spectra exhibit a very similar spectral shape across the different regions. Absorption at 443 nm ranges from 0.02 to 0.06 $m^2.mg^{-1}$. Some regions display particularly strong and well-defined peaks, such as the Med Sea 3 at 443 and 675 nm. In contrast, regions such as the English Channel and the Baltic Sea exhibit flatter spectra and lower mean a_{PHY}^* (443) values (0.02 & 0.03 $m^2.mg^{-1}$) (Table 3). In these regions, the characteristic absorption features appear less clearly defined compared with the other areas (Fig. 5).

Variations in the magnitude of a_{PHY}^* and the definition of spectral peaks reflect intra and interregional variability in the size structure of phytoplankton communities and physiological photo-acclimation. Indeed, regions with a flatter spectral shape exhibit high TChla values. This is characteristic of productive waters, where phytoplankton assemblages are generally dominated by larger taxa (e.g. diatoms), leading to a stronger packaging effect and reduced chlorophyll-specific absorption such as the English Channel.

In the Baltic Sea, the picoplankton fraction is higher than the other fractions. However, in this region, filamentous cyanobacteria can be observed during summer blooms, which lead to errors in fraction identification (Stal et al., 2003; Olofsson et al., 2020). Despite a pigment signature dominated by zeaxanthin, typically associated with picoplankton, these cyanobacteria form filamentous and colonial structures reaching hundreds of micrometers to millimeters in length. Indeed, filamentous cyanobacteria form long filaments or aggregates and act as a microplankton fraction. This shift in scale induces an extreme packaging effect driven by mutual shading of pigments within the filaments. As a result, internal pigments are optically masked by outer layers which may explain the flatter spectral shape. This explains why standard size-based models are expected to fail in such conditions (Brewin et al., 2010). This is consistent with the sampling period (June–July), which coincides with summer blooms in the Baltic Sea.

Conversely, the Med Sea regions (Med Sea 2 and 3) exhibit low TChla values which are characteristic of oligotrophic waters. However, these regions do not reach the high absorption coefficient predicted by the B95 model. This discrepancy suggests an anomalously high packaging effect for low-biomass waters. Indeed, according to the B95 model by Bricaud et al. (1995), low TChla values are associated with the dominance of small phytoplankton cells which are supposed to absorb light very efficiently due to their reduced packaging effect. This leads to higher predicted light absorption values given by the B95 model.

https://doi.org/10.5194/egusphere-2026-4579
Preprint. Discussion started: 7 September 2026

However, the study by Pérez et al. (2021) shows that reality is more complex. Indeed, the Mediterranean Sea is driven by photo-acclimation induced by high solar irradiance and marked stratification. This stratification leads to the formation of a pronounced thermocline, which vertically structures the water column into a distinct physiological compartment. This mechanism leads to a change in the pigment density maintaining a significant packaging effect despite the small physical size of the cells, through an increase in intracellular pigment concentration, resulting in absorption values lower than expected (Organelli et al., 2017). As a consequence, this induces a decoupling between phytoplankton size structure and optical absorption properties, explaining why the B95 model fails to capture the observed variability.

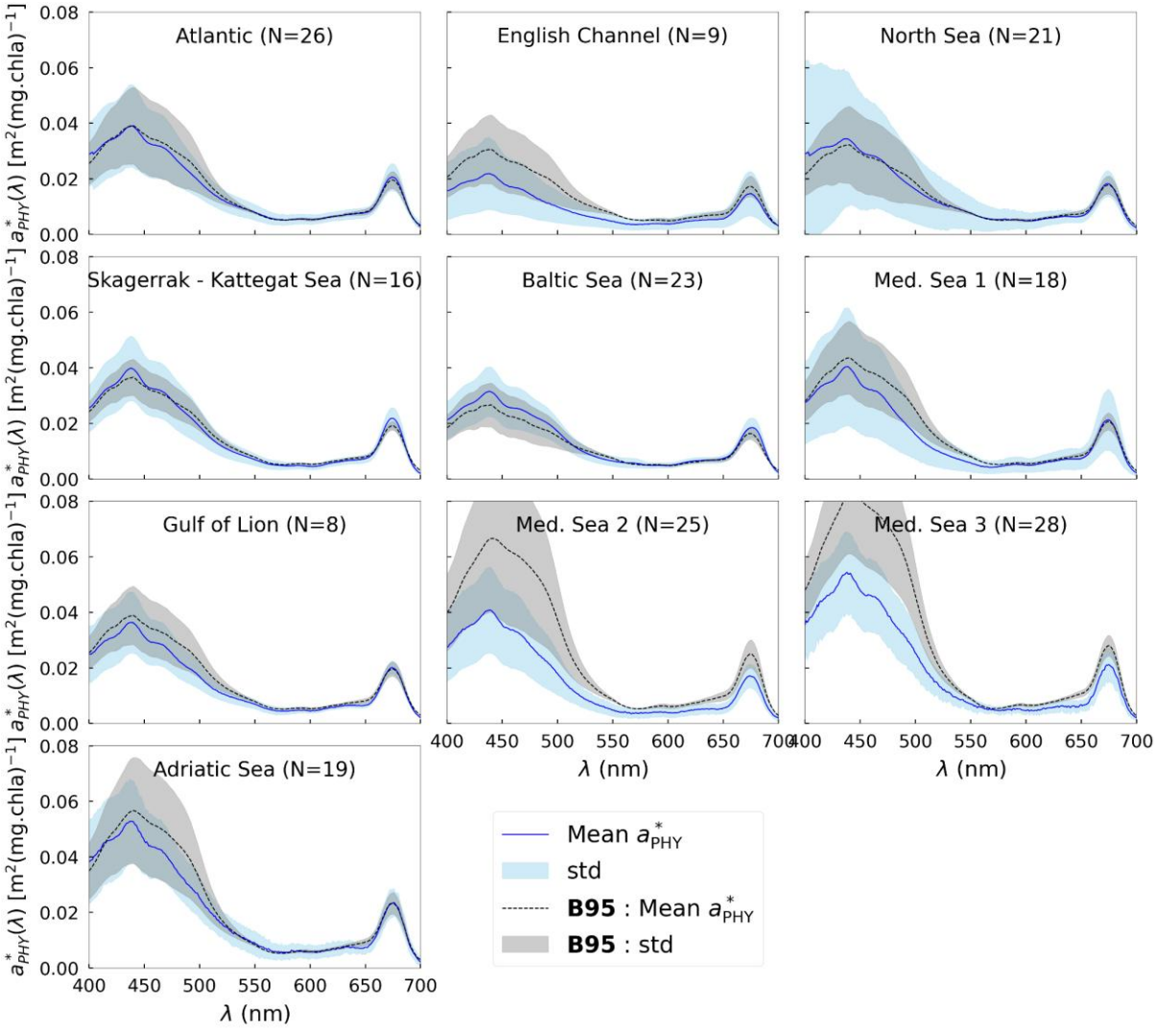

Figure 5: Representation of the mean of the specific light absorption coefficient by phytoplankton (blue line) by region between 400 and 800 nm with standard deviation. Statistics of Bricaud et al. (1995) is in dashed black line.

https://doi.org/10.5194/egusphere-2026-4579
Preprint. Discussion started: 7 September 2026

Table 3. Summary statistics (mean ± SD, range) of $a_{PHY}^*(443)$ by region.

Region	a_{PHY}*(443) [m^2 (mg Chla)$^{-1}$]	
	Mean ± SD	Range
Atlantic (N = 29)	0.037 ± 0.014	0.009 – 0.060
English Channel (N = 9)	0.020 ± 0.012	0.002 – 0.035
North Sea (N = 22)	0.032 ± 0.022	0.008 – 0.121
Skagerrak – Kattegat Sea (N = 16)	0.037 ± 0.011	0.023 – 0.068
Baltic Sea (N = 23)	0.030 ± 0.008	0.018 – 0.046
Med. Sea 1 (N = 19)	0.038 ± 0.020	0.006 – 0.094
Gulf of Lion (N = 8)	0.034 ± 0.010	0.023 – 0.050
Med. Sea 2 (N = 25)	0.038 ± 0.014	0.003 – 0.065
Med. Sea 3 (N = 30)	0.051 ± 0.014	0.025 – 0.084
Adriatic Sea (N = 21)	0.049 ± 0.013	0.027 – 0.076

The phytoplankton absorption coefficient (a_{PHY}) at 6 selected wavelengths corresponding to the MEdium Resolution Imaging Spectrometer (MERIS) and Ocean and Land Colour Instrument (OLCI) spectral (Rast et al., 1999; Doerffer and Schiller, 2007; Donlon et al., 2012; Atwood et al., 2024) is compared with the empirical power-law relationships and 90 % confidence intervals established by Bricaud et al. (1995) (B95; dashed line) (Fig. 6). Values follow a highly predictable trend and show strong consistency with the B95 model, with the majority of data points falling within the 90 % confidence intervals. At low TChla concentrations, values tend to be close to the lower confidence interval whereas at high TChla concentrations they are closer to the upper confidence interval. In the Baltic Sea, values tend to cluster near the upper confidence limit, suggesting high absorption efficiency. Some values can be observed below the B95 statistics. The majority of these values are observed in the Med Sea (Med Sea 1 and Med Sea 2) at 490 and 510 nm. However, some points below the B95 statistics are also observed for other wavelengths and regions. In the English Channel, the stations with the highest TChla concentrations (3 stations) present lower phytoplankton absorption coefficients. Some regions show a very good agreement with the model and do not cross the statistical limits. The Atlantic Ocean and the Skagerratt-Kattegat Sea present very stable values that remain within the expected range.

https://doi.org/10.5194/egusphere-2026-4579
Preprint. Discussion started: 7 September 2026

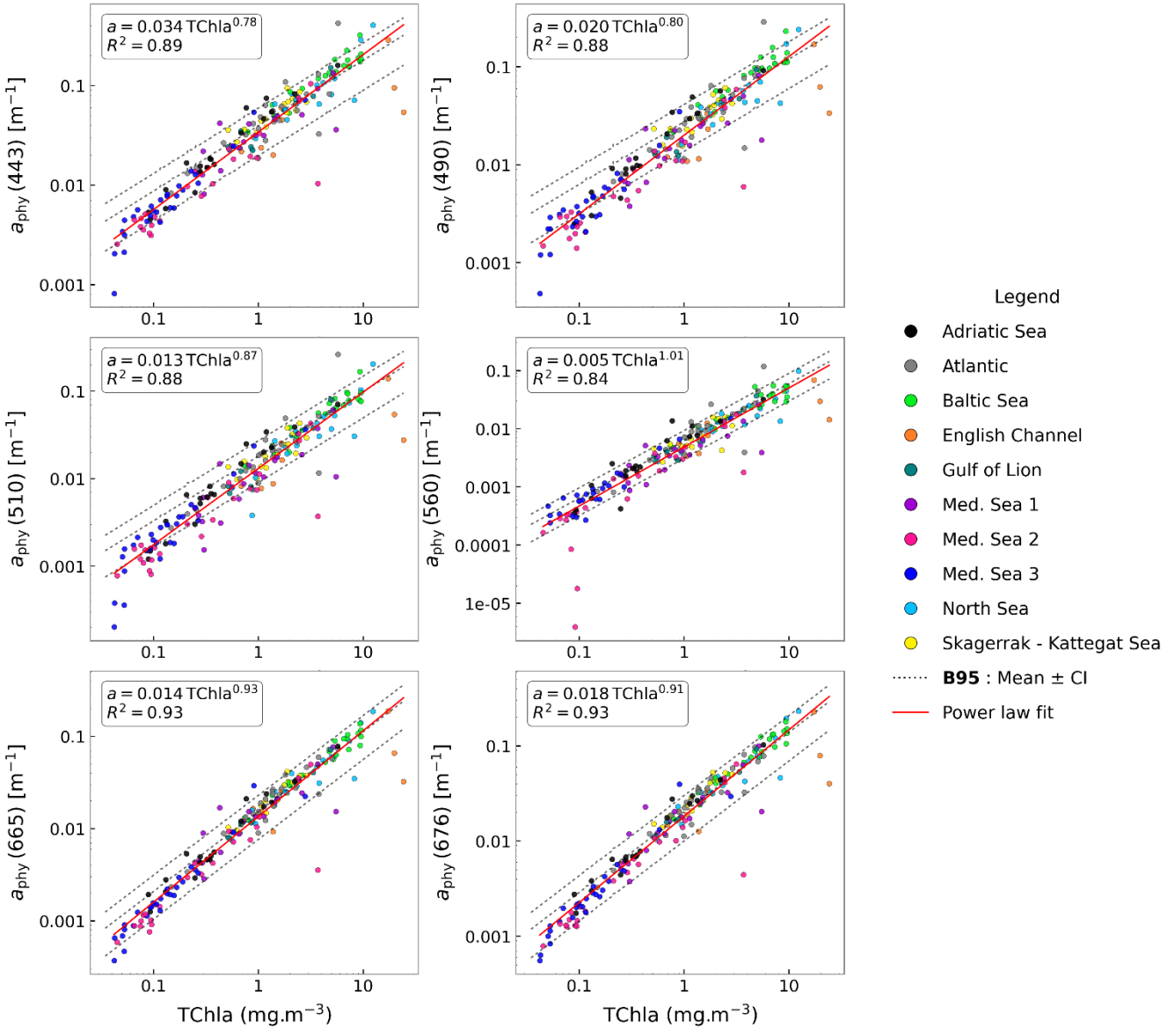

Figure 6: Scatterplots of the phytoplankton absorption coefficient in function of TChla at 6 different reference wavelengths with representation of B95 statistics obtained with Bricaud et al.(1995) in dashed lines.

415 Phytoplankton size fractions vary across European coastal waters according to TChla concentrations as estimated using the Chase et al. (2020) and the new parameterizations (Fig. 7). Overall, both parameterizations reproduce similar large-scale spatial patterns in pigment-derived phytoplankton size structure across European coastal waters, with increasing relative microplankton contributions and decreasing relative picoplankton contributions as TChla increases. However, the estimated relative contributions of the three size classes differ substantially between the two models.

https://doi.org/10.5194/egusphere-2026-4579
Preprint. Discussion started: 7 September 2026

Compared with the parameterization of Chase et al. (2020), the new coastal parameterization generally predicts higher picoplankton contributions, frequently exceeding 40 % and reaching up to 60 % (Fig. 7a). It also estimates lower nanoplankton contributions, which remain relatively stable (20–40 %) across the full range of chlorophyll values (Fig. 7b). In contrast, the Chase et al. (2020) parameterization predicts higher nanoplankton contributions (40–80 %, Fig. 7e) and lower maximum picoplankton contributions (up to approximately 40 %, Fig. 7d). Similarly, while both parameterizations indicate increasing microplankton contributions with increasing TChla, the coastal parameterization predicts much larger maximum contributions (up to 80–100 %, Fig. 7c), whereas the Chase et al. (2020) parameterization rarely exceeds 50 % (Fig. 7f). This new coastal parameterization predicts microplankton-dominated communities in the North Sea and the English Channel (up to 80–100 %), consistent with their relatively high chlorophyll concentrations (eutrophic conditions). Inversely, the Mediterranean regions (Med Sea 2 and Med Sea 3) are predicted to be dominated by picoplankton (up to 60 %), reflecting the low Chla concentrations characteristic of the Mediterranean Sea (oligotrophic conditions).

The Baltic Sea exhibits a distinct behavior with both parameterizations. Despite relatively high TChla concentrations, the predicted phytoplankton size structure differs from that expected for productive waters. The coastal parameterization estimates unusually high picoplankton contributions, whereas the Chase et al. (2020) parameterization predicts nanoplankton dominance together with relatively elevated picoplankton contributions. This pattern may be related to the dominance of filamentous cyanobacteria (Aphanizomenon sp.) during summer blooms (Olofsson et al., 2020). Although these organisms contain zeaxanthin, a pigment commonly used as a biomarker for picoplankton, they form filaments and aggregates reaching several millimeters in length (van Dijk et al., 2010), placing them outside the picoplankton size range. Consequently, the correspondence between diagnostic pigments and phytoplankton size classes may break down under these conditions, leading to potentially biased size-fraction estimates from pigment-based parameterizations (Brewin et al., 2010).

The differences between the two parameterizations illustrate the sensitivity of pigment-based estimates of phytoplankton size structure to the model. Although the parameterization of Chase et al. (2020) was evaluated against flow cytometry observations, both approaches infer size fractions indirectly from diagnostic pigments.

https://doi.org/10.5194/egusphere-2026-4579
Preprint. Discussion started: 7 September 2026

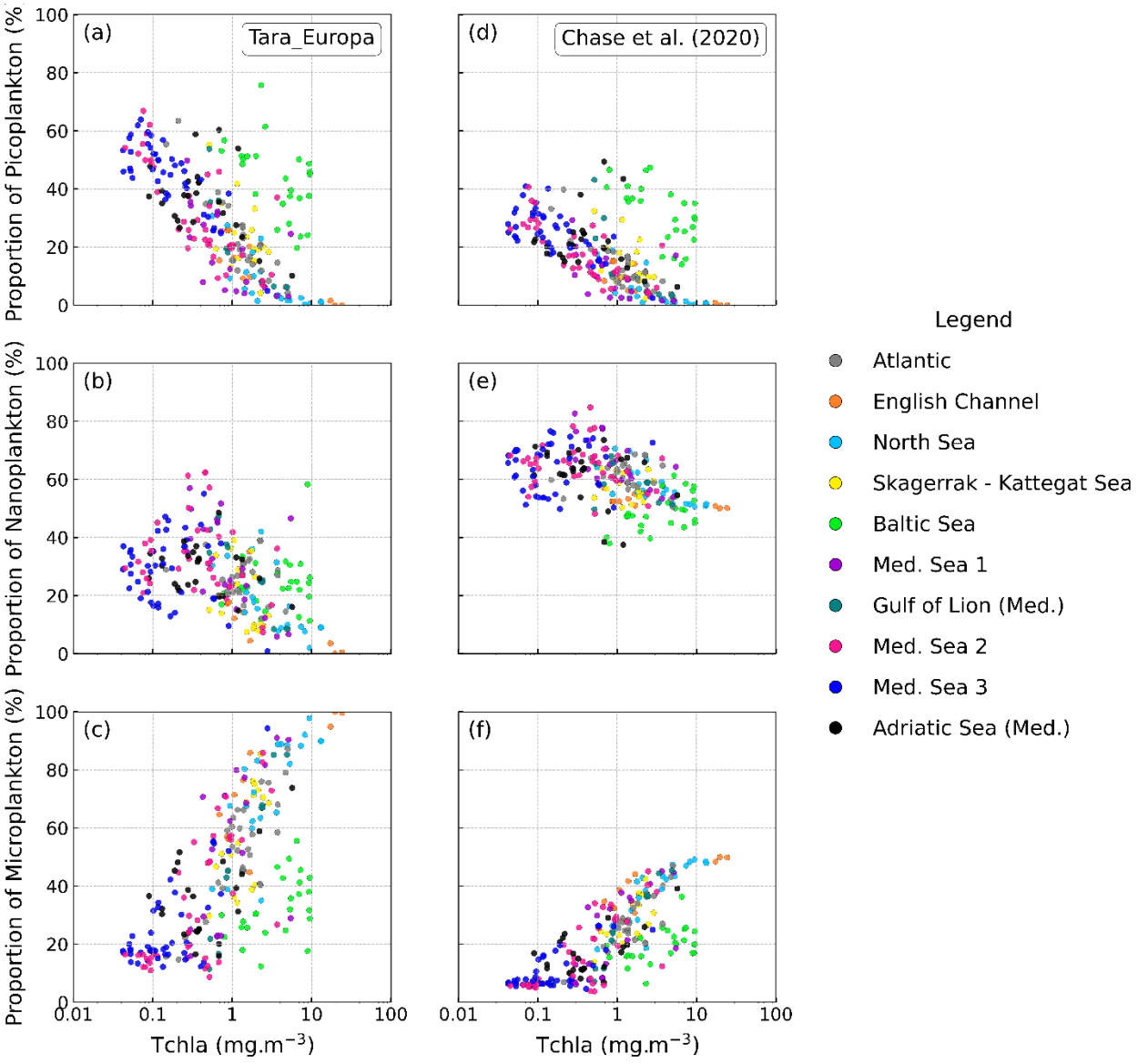

Figure 7: Variability of (a,d) picoplankton, (b,e) nanoplankton, and (c,f) microplankton proportions as a function of TChla obtained using the new parametrization for coastal waters (left) and the parametrization by Chase et al. (2020) (right) (Table 1).

Phytoplankton light absorption coefficients at 443 exhibit substantial variability as a function of the coefficient at 676 nm (Fig. 8a). The absorption coefficients range from 0.001 m^{-1} to 0.5 m^{-1}. The relationship between these two absorption peaks follows a tight power law, close to the one predicted by Bricaud et al. (1995). It appears as a linear relationship in log–log space, with $a_{PHY}(443)$ is generally higher than $a_{PHY}(676)$ especially at low biomass (ratio higher at low biomass than at high biomass). For the 443:676 ratio (Fig. 8b), the data are scattered around the B95 relationship, the dispersion appears more limited than that reported by Babin et al. (2003b). Several observations fall below the regression line at low TChla concentrations. While Babin

https://doi.org/10.5194/egusphere-2026-4579
Preprint. Discussion started: 7 September 2026

et al. (2003b) reported significant regional variability for European seas relative to the B95 model, the present data shows a relatively limited dispersion. At concentrations below 0.1 mg m^{-3}, the 443:676 ratio exhibits its maximum range of variation, with values spreading both above and below the B95 mean. The data follow the general decreasing trend of the blue-to-red absorption ratio with increasing biomass, as predicted by the B95 model.

The first relationship between the phytoplankton absorption coefficients at 443 nm and 676 is driven essentially by biomass expressed as total TChla. Indeed, TChla contributes to both spectral peaks $a_{PHY}(443)$ and $a_{PHY}(676)$ and evolves similarly at these two wavelengths. In this comparison, the biomass signal masks secondary physiological factors such as pigment composition or community size structure.

While absolute absorption coefficients are primarily driven by the biomass (TChla), the 443:676 ratio reduces this dominant effect, allowing secondary factors such as pigment composition and packaging effects to emerge (Bricaud et al., 2004). According to the B95 model, the ratio decreases as TChla increases. This theoretical decrease is predicated on a global ecophysiological transition: at low TChla, Bricaud et al. (1995) hypothesize that waters are always dominated by small cells with high accessory pigment content and minimal packaging, and inversely at high TChla.

In reality, waters can evolve completely differently and natural populations can diverge from the average trend due to regional specificities in community structure. The packaging effect varies spectrally, having a stronger effect at $a_{PHY}(443)$. In this study, the majority of ratio values (TChla > 1 mg m^{-3}) fall below the B95 regression line may indicate enhanced packaging effect or shifts in phytoplankton community structure (Fig. 8b). This discrepancy suggests a dominance of large phytoplankton cells or an unusually high intracellular pigment density which limit the expansion of the 443 nm peak and result in lower-than-predicted ratios.

https://doi.org/10.5194/egusphere-2026-4579
Preprint. Discussion started: 7 September 2026

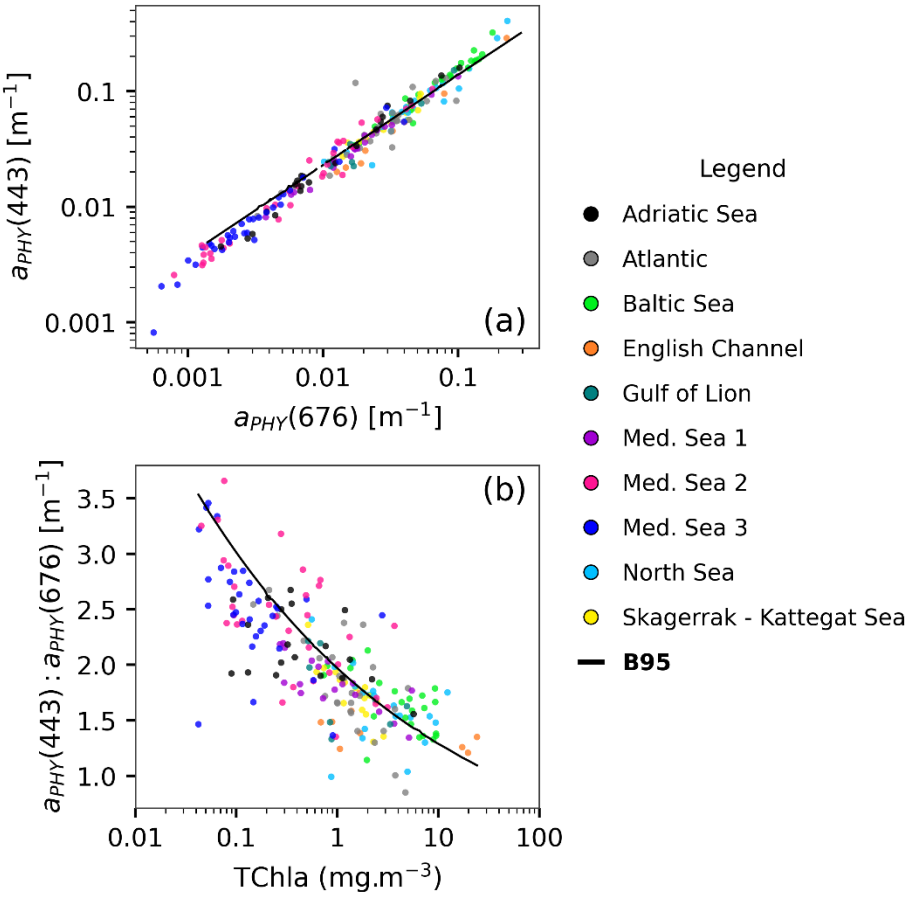

Figure 8: (a) Variations of the light absorption coefficients of phytoplankton at 443 in function of the coefficient at 676 nm (b) and ratio 443:676 as a function of total chlorophyll a (TChla). The black lines are the regression lines obtained from the model of Bricaud et al. (1995).

3.4. Non-Algal Particle Absorption

Non-algal particles (NAP) consist of organic materials (e.g. bacteria), detritus and minerogenic matter. These constituents play a fundamental role in shaping the underwater light field. Unlike in offshore waters, NAP concentrations in coastal environments vary independently of phytoplankton biomass highlighting the optically complex nature (Babin et al., 2003b; Spyrakos et al., 2018). Light absorption follows an exponential form similar to that of CDOM. The spectral slope can be used as a proxy for the nature and size distribution of particle assemblages (Woźniak et al., 2024). The specific light absorption coefficient (a_{NAP}^{*}) further provides insight into the optical efficiency of these particles. Moreover, this study addresses the limitations of historical "null-point" corrections by accounting for non-negligible NAP absorption in the near-infrared (NIR) region (Röttgers et al., 2014).

https://doi.org/10.5194/egusphere-2026-4579
Preprint. Discussion started: 7 September 2026

Mean mass-specific light absorption spectra between 400 and 700 nm for NAP (a_{NAP}^*) exhibit a consistently similar spectral shape across the ten regions studied (Fig. 9). Spectra follow an exponentially decreasing function and present a maximum at 400 nm and a minimum at 700 nm. Beyond 700 nm, in the NIR, absorption remains measurably non-zero and presents a significant offset (dashed red lines). This contradicts the historical "null-point correction" (setting absorption to zero at 750 nm), which can lead to an underestimation of particulate absorption by up to 30 % in the blue and 80 % in the red according Röttgers et al. (2014) (Fig. 11). The maximum absorption values (at 400 nm) range from 0.03 to 0.08 $m^2 g^{-1}$ and the minimum absorption values (at 700 nm) range from 0.002 to 0.009 $m^2 g^{-1}$. Some regions present a high intra-regional variability such as Med Sea 3. A clear regional gradient with increasing values is observed from the Atlantic to the Baltic Sea. The Baltic Sea exhibits the highest absorption values, with an average for a_{NAP}^* (443) of 0.057 $m^2 g^{-1}$, which is nearly twice as high as the other European coastal regions (between 0.02 $m^2 g^{-1}$ for the Adriatic Sea and 0.057 $m^2 g^{-1}$ for the Baltic Sea, Table 4).

The magnitude of a_{NAP}^* is driven by particle size, composition, and riverine inputs (Estapa et al., 2012). Organic particles generally exhibit higher specific absorption than mineral ones. The same variations were observed by Babin et al. (2003b) and Pitarch and Brando (2025). This is well illustrated by the classification of Spyrakos et al. (2018), who identified a specific category for turbid waters with high organic content (OWT4). These waters exhibit high specific absorption by NAP. This highlights that an increase in the organic fraction of the total suspended matter leads to a more efficient light absorption per unit of mass.

In the Baltic Sea, high specific absorption (0.08 $m^2 g^{-1}$ at 400 nm) is observable which is driven by the relatively high organic content of the suspended particulate pool. Indeed, the Baltic Sea can be classified as a water type of OWT4 (Spyrakos et al., 2018). Moreover, in this region, the majority of stations present a POC:SPM ratio >25 % (Fig. 1b) and according to Tran et al. (2019), such values are representative of organic dominated waters where particulate assemblages are dominated by organic particles. This organic content is consistent with the elevated CDOM concentrations. The predominance of organic particles enhances light absorption. Similar conditions are responsible for high specific absorption in the North Sea. Additionally, terrigenous inputs in the Skagerrak Sea may supply iron-rich mineral assemblages, which significantly boost absorption independently of the organic carbon pool (Estapa et al., 2012).

In the literature, the Mediterranean Sea is considered a dominantly organic environment (Bengil et al., 2016; Zibordi and Berthon, 2024) and should therefore exhibit high absorbance values. However, the reality is more complex in coastal waters. Indeed, the Gulf of Lion presents the highest absorbance among all Mediterranean sub-basins despite its inorganic character (many stations exhibit a POC:SPM ratio near 6 %, Fig 3b). These absorbance values could be explained by the presence of iron oxides, as observed in the Skagerrak Sea. Indeed, the presence of iron oxides significantly increases absorption in the blue-green range (Estapa et al., 2012). For the Gulf of Lion, the Rhone River acts as a major source of these iron-rich minerals (Babin and Stramski, 2004; Bégorre et al., 2022).

https://doi.org/10.5194/egusphere-2026-4579
Preprint. Discussion started: 7 September 2026

In other Mediterranean sub-basins, absorption is relatively lower despite high organic content (Bengil et al., 2016; Zibordi and Berthon, 2024). Indeed, many stations present POC:SPM ratio values higher than 25 % (Fig. 3b) in some sub-basins (Med. Sea 1, Med. Sea 3 and Adriatic Sea). In this case, this could be due to the presence of old organic particles. Indeed, older organic matter absorbs light less efficiently. Old organic matter has lost its chromophores by photodegradation or bacterial degradation, which leads to decrease in its light absorption efficiency compared to fresh organic matter (Pitarch and Brando, 2025).

Moreover, according to Babin et al. (2003b), this can also be attributed to methodological normalization bias. Indeed, the method used to derive a_{NAP}^{*} may introduce bias. In phytoplankton-dominated waters, the mass of living algae is included in the SPM (denominator), whereas their major pigments are removed with MeOH to measure a_{NAP} (numerator); This mismatch between the absorption and mass pools leads to artificially lowering the resulting specific absorption value (a_{NAP}^{*}). This effect remains weaker in coastal waters where minerals and non-algal detritus dominate the total particle mass (Babin et al., 2003b). In addition, pigment extraction does not necessarily remove all phytoplankton-derived absorption, as some colored compounds derived from phytoplankton may remain after extraction. These residual compounds may contribute to the light absorption by non-algal particles (a_{NAP}).

https://doi.org/10.5194/egusphere-2026-4579
Preprint. Discussion started: 7 September 2026

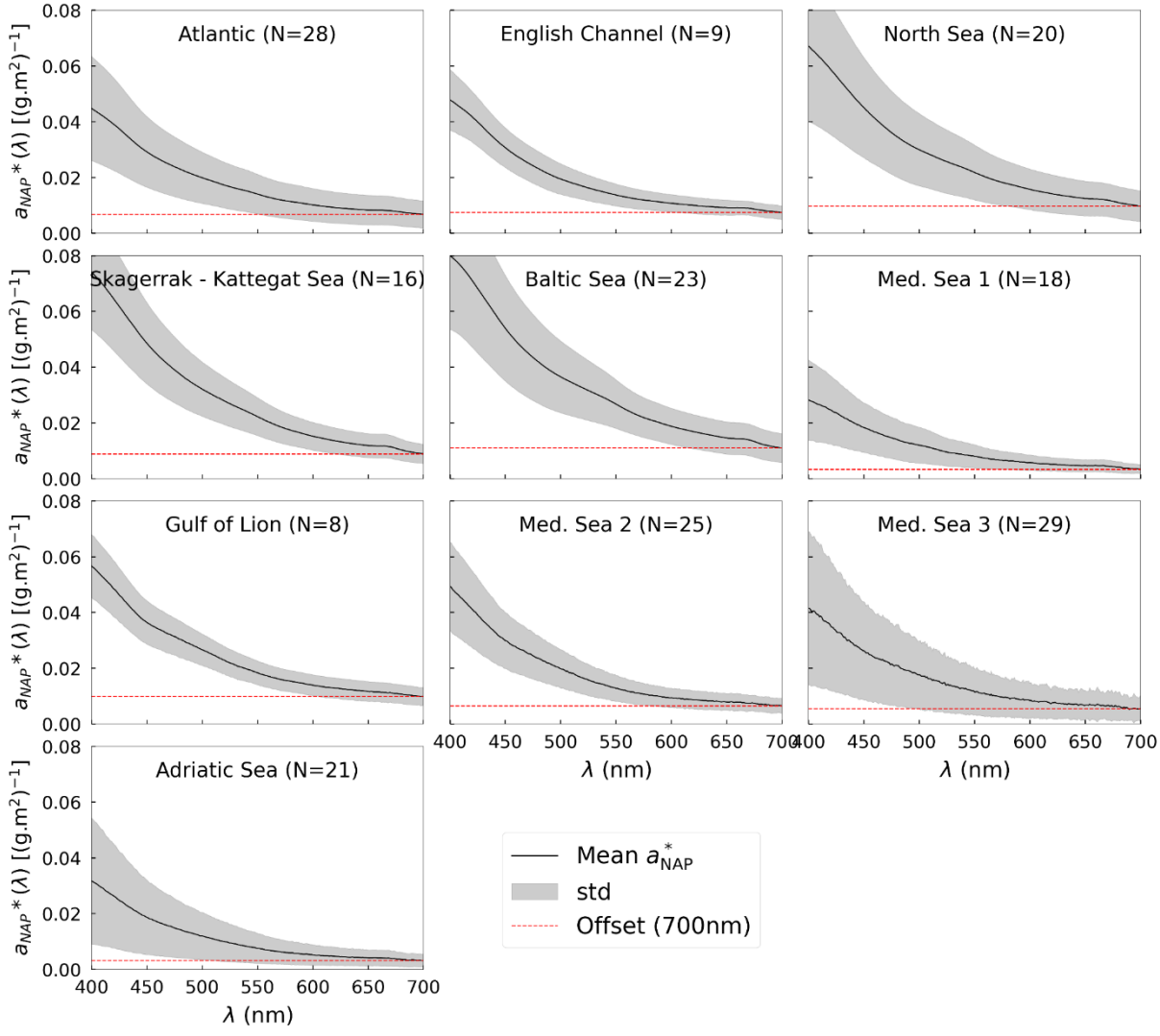

Figure 9: Mean non-algal particle mass-specific absorption coefficient spectra (a_{NAP}*=a_{NAP}/SPM) by region from 400 to 800 nm with standard deviation. Red horizontal lines indicate the NIR absorption offset.

Table 4. Summary statistics (mean ± SD, range) of a_{NAP}*(443) by region and regional S_{NAP} values derived from exponential fits (Eq. 9) to $a_{NAP}(\lambda)$. Standard deviations of S_{NAP} represent spatial variability among stations within each region, are reported.

	a_{NAP}*(443) [m² g⁻¹]		S_{NAP} (nm⁻¹)	
Region	Mean ± SD	Range	Mean ± SD	Range
Atlantic (N = 29)	0.031 ± 0.013	0.008 – 0.055	0.010 ± 0.001	0.008 – 0.012
English Channel (N = 9)	0.032 ± 0.007	0.020 – 0.040	0.011 ± 0.001	0.010 – 0.011

https://doi.org/10.5194/egusphere-2026-4579
Preprint. Discussion started: 7 September 2026

North Sea (N = 22)	0.045 ± 0.020	0.012 – 0.086	0.010 ± 0.001	0.008 – 0.011
Skagerrak – Kattegat Sea (N = 16)	0.051 ± 0.015	0.025 – 0.081	0.010 ± 0.001	0.009 – 0.011
Baltic Sea (N = 23)	0.057 ± 0.020	0.022 – 0.094	0.009 ± 0.001	0.007 – 0.011
Med. Sea 1 (N = 19)	0.020 ± 0.009	0.005 – 0.035	0.010 ± 0.001	0.009 – 0.011
Gulf of Lion (N = 8)	0.038 ± 0.008	0.028 – 0.052	0.010 ± 0.000	0.009 – 0.011
Med. Sea 2 (N = 25)	0.031 ± 0.010	0.015 – 0.054	0.011 ± 0.001	0.010 – 0.013
Med. Sea 3 (N = 30)	0.028 ± 0.019	0.004 – 0.083	0. 011 ± 0.001	0.009 – 0.012
Adriatic Sea (N = 21)	0.020 ± 0.014	0.002 – 0.063	0. 011 ± 0.001	0.010 – 0.012

A strong linear relationship is observed between a_{NAP} at 443 nm and the suspended particulate matter (SPM) concentration (Fig. 10a). A robust linear regression ($R^2 = 0.94$) was established across three orders of magnitude with SPM concentrations ranging from 0.1 to 100 g m^{-3}. The regression was forced through the origin to maintain physical consistency. The slope obtained is 0.0249 for this dataset. This value is highly consistent with previous studies and falls between the slope average value of 0.0235 reported by Bowers et al. (1996)) and the average value of 0.031 established by Babin et al. (2003b) for European coastal waters.

The range of S_{NAP} values, calculated using a non-linear exponential model fitted to the dataset, is shown in Fig. 10b. The mean average value found is 0.0102 nm^{-1} for a total of 201 samples. The S_{NAP} values range from 0.007 to 0.013 nm^{-1} with the lowest value found in the Baltic Sea and the highest value in Med Sea 3 (Table 4). Across regions, S_{NAP} values are very similar and do not show strong variations. They remain relatively constant, region averages range from 0.009 for the Baltic Sea to 0.011 nm^{-1} for some regions in the Med Sea such as Med Sea 2, Med Sea 3 or Adriatic Sea. S_{NAP} values in this study are lower than those reported by Babin et al. (2003b).

This difference can be explained by the use of an offset. Babin et al. (2003b) assumed that non-algal particles do not absorb in the NIR and constrained the model to reach zero in the NIR, which artificially increases S_{NAP} values. This assumption is likely incorrect. According to Röttgers et al. (2014), non-algal particles absorb a non-negligible value in the NIR. Therefore, S_{NAP} values are expected to be lower. However, values are really similar to those reported by Zibordi and Berthon (2024) who observed regional averages ranging from 0.009 to 0.013 nm^{-1}. Bowers and Binding (2006) also found a global average of 0.012 nm^{-1} which is consistent with this study. Both of these studies used an offset for the exponential fit.

While the majority of stations follow a predictable trend, some extreme values are observed in different environments. Low S_{NAP} values are observed in the Baltic Sea (0.007 nm^{-1}). These values provide insights into the particle quality. However, according to Röttgers et al. (2014), the contribution of the detrital organic pool to NIR absorption remains largely unknown, while mineral particles are proven NIR absorbers. Therefore, these lower values suggest even minor mineral inputs or specific organo-mineral complexes could drive differences in light absorption efficiency and modify spectral expansion. Such cases

https://doi.org/10.5194/egusphere-2026-4579
Preprint. Discussion started: 7 September 2026

demonstrate that in transition waters, the interaction between organic matter and mineral cores (e.g., through flocculation) is a primary driver of spectral expansion and NIR magnitude.

Moreover, flocculation process is mostly common in this region and can drive little particles to large particles which contribute to the NAP pool. This consequently leads to flatter spectra and lower S_{NAP} values (Stramski et al., 2007).

In contrast, some stations in the Med Sea exhibit high S_{NAP} values (up to 0.013 nm^{-1}). One possible explanation is a greater contribution of small particles. Indeed, very small particles (colloids) are not significantly affected by the packaging effect and absorb light more efficiently, increasing the spectral expansion and resulting in higher S_{NAP} values (Stramski et al., 2007).

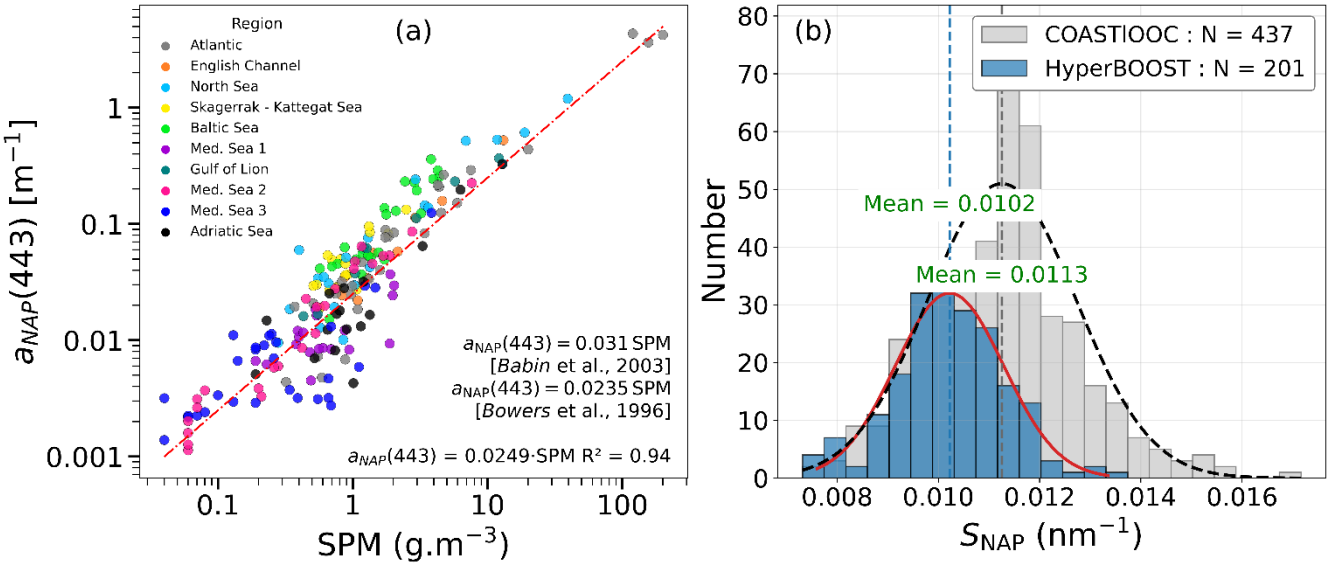

Figure 10: (a) Variability of $a_{NAP}(443)$ as a function of SPM concentration. The dashed red line represents the linear regression with null intercept. (b) Frequency distribution of the spectral slope (S_{NAP}) found between 380 and 730 nm for both datasets, with Gaussian curve shown in red for the HyperBOOST dataset and in black for the COASTlOOC dataset.

A positive correlation is observed between the spectral ratio of particulate absorption at 750 nm to 443 nm and the absorption at 750 nm (Fig. 11a). The ratio increases when the particulate absorption in the NIR also increases. This ratio reaches a maximum level of 0.3 (30 %), i.e. absorption in the NIR represents 30 % of the absorption at 443 nm by all particles. However, the majority of values stay between 0.01 (1 %) and 0.1 (10 %). Maximum values are reached by some stations in the Atlantic, such as in the Gironde estuary.

Another positive correlation is shown between the spectral ratio of particulate absorption at 750 to 672 nm and the absorption at 750 nm (Fig. 11b). Ratio values reach a maximum value at 0.8 (80 %). Absorption in the NIR represents 80 % of the absorption at 672 nm for all particles. However, the majority of values stay between 0.05 (5 %) and 0.5 (50 %).

In each graph, a large intra-regional variability is observed. These graphs confirm that it is important to consider absorption in the NIR. The non-linear trends suggest that variability does not depend only on particle concentration but also on the quality

https://doi.org/10.5194/egusphere-2026-4579
Preprint. Discussion started: 7 September 2026

of particles (Röttgers et al., 2014). According to Babin and Stramski (2004), mineral colored particles and sediments increase efficiency of the absorption. Furthermore, the absorption efficiency is modulated also by the particle size distribution; smaller particles exhibit higher mass-specific absorption due to a reduced packaging effect compared to larger particles (Stramski et al., 2007).

It is possible to observe a gradient from the Med Sea to the Atlantic Ocean. Regions in the Med Sea present lower ratios than the Atlantic Ocean (up to 30 % for the first ratio and 80 % for the second ratio). Particularly, maximum ratios are observed in the Atlantic Ocean (stations located at the end of estuaries), while minimum ratios are observed in Med Sea 1. However, Med. Sea 3 and even Med. Sea 2 seem to deviate from the regression.

These results confirm and provide further evidence for the limitations of the traditional 'null-point correction' at 750 nm for particulate absorption by Tassan and Ferrari (1995, 2003). As demonstrated by Röttgers et al. (2014), this correction is invalid in turbid waters and leads to a substantial underestimation of the particulate absorption budget.

https://doi.org/10.5194/egusphere-2026-4579
Preprint. Discussion started: 7 September 2026

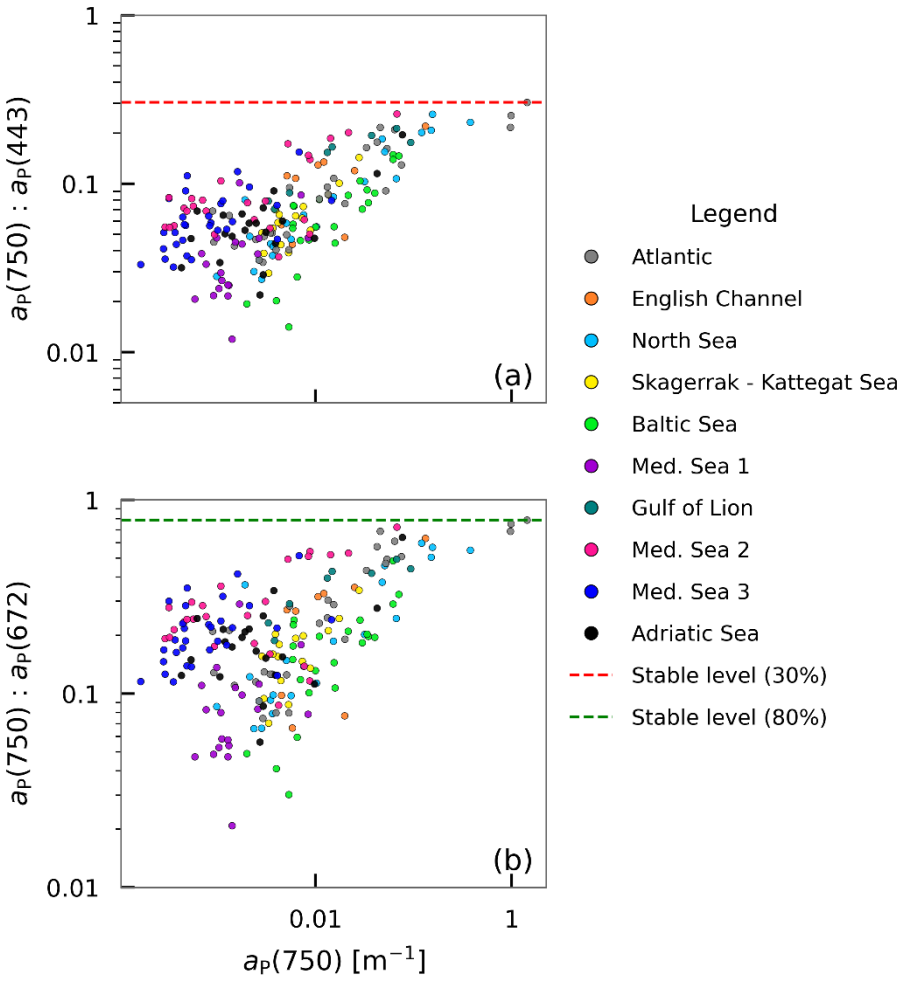

Figure 11: Representation of different spectral ratios of the particulate absorption: (a) 750 nm to 443 nm ($a_P(750):a_P(443)$) and (b) 750 nm to 672 nm ($a_P(750):a_P(672)$) as a function of $a_P(750)$ for all studied regions. The horizontal dashed lines mark ratios corresponding to 30 % of $a_P(443)$ in panel (a) and 80 % of $a_P(672)$ in panel (b).

3.5. Absorption Budget

The relative contributions of Chla, NAP and CDOM to light absorption in natural waters can be illustrated by ternary plots. This triangular classification was introduced by Prieur and Sathyendranath (1981).

The contribution of the three optically-active water constituents to water absorption across wavelengths is shown in Fig. 12. Different dominant regimes can be identified. In the near UV, in the 380-412 nm range, CDOM is the dominant contributor (between 40 % and 100 %). CDOM exhibits maximum absorption in this spectral region. This contribution decreases toward the NIR region. In the 490-560 nm range, absorption is dominated by CDOM and NAP (each contributing up to 80 %). At 620 nm, all particles exhibit similar contributions. No single component dominates waters. The relative contribution of CDOM

https://doi.org/10.5194/egusphere-2026-4579
Preprint. Discussion started: 7 September 2026

significantly decreases, reaching average values between 14 % and 24 %. While CDOM is no longer the dominant component as it is in the UV-blue range, its contribution remains non-negligible in the red part of the spectrum. Consequently, absorption in this range is primarily driven by NAP and phytoplankton, though CDOM must still be accounted for to accurately balance the absorption budget.

615 However, at 665 and 676 nm, phytoplankton dominate absorption over non-algal particles (in most cases, between 60 % and 100 %). Conversely, at 709, absorption is exclusively attributed to NAP (in most cases, between 60 % and 100 %). In particular, this is representative of a baseline offset.

The regions are highly mixed, making it difficult to distinguish differences in contributions. However, it is possible to observe that some regions in the Atlantic and the North Sea consistently show NAP dominance. These stations are typically located in

620 front of estuaries.

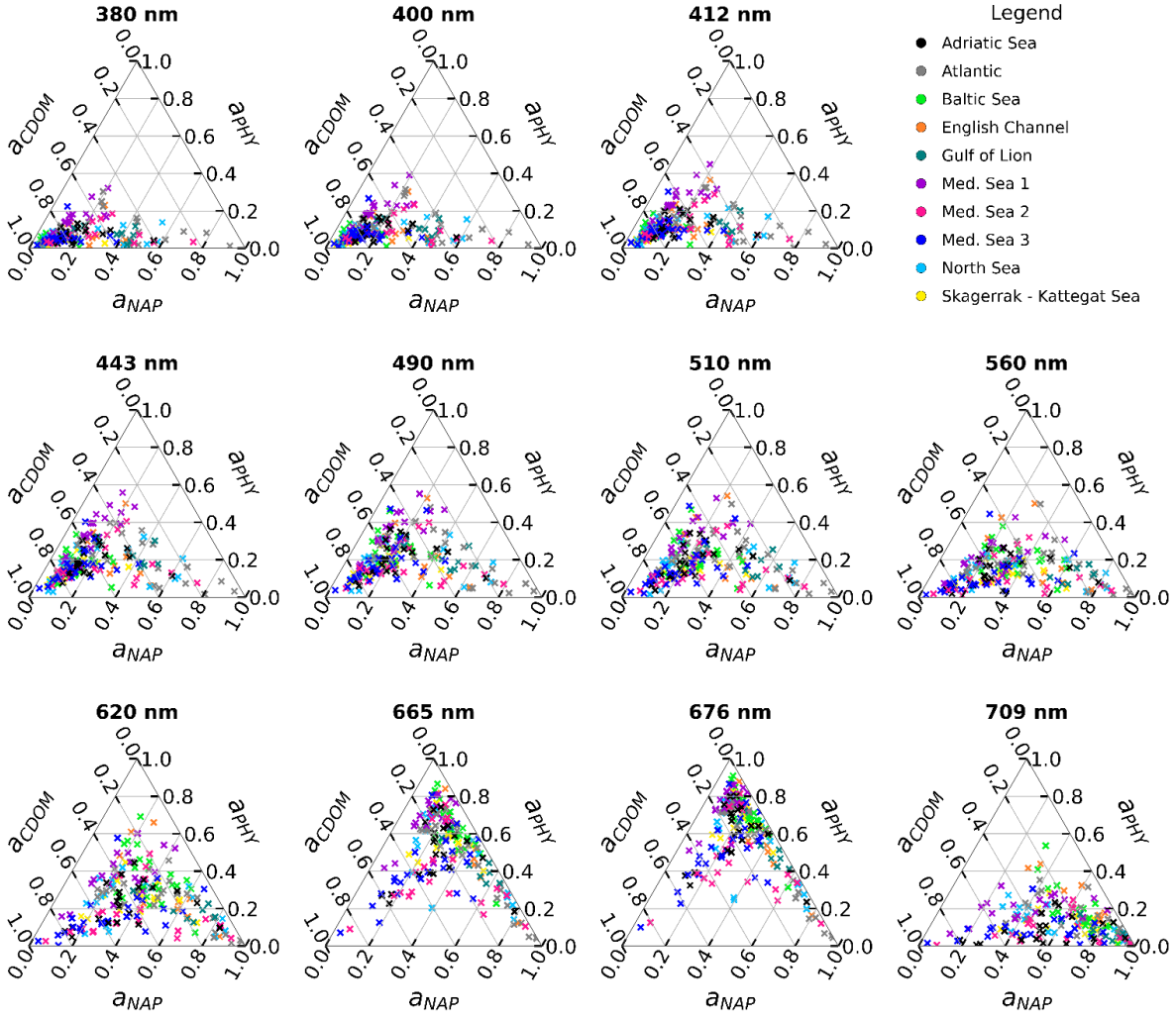

https://doi.org/10.5194/egusphere-2026-4579
Preprint. Discussion started: 7 September 2026

Figure 12: Ternary plots illustrating the respective contributions of surface CDOM, phytoplankton (Chla) and NAP to total non-water absorption at 11 wavelengths.

4. Conclusion & Perspectives

This study provides a comprehensive in situ biogeochemical and light absorption dataset collected over two years in European coastal waters, with 202 stations sampled from the Baltic Sea to the Mediterranean Sea. This dataset extends previous studies conducted in European coastal waters, including those of Babin et al. (2003b), Zibordi and Berthon (2024), and Pitarch and Brando (2025). It benefits from methodological advances compared with previous studies, including improved instrumentation and measurement protocols. In particular, particulate absorption was determined using an integrating sphere, whereas the transmittance–reflectance technique was employed in Babin et al. (2003b). However, the dataset also presents some limitations. As each station was sampled only once, seasonal variability was not assessed (it will be in the starting SUPPaCOOL ESA project).

Light absorption by CDOM reveals distinct regional and compositional patterns. CDOM spectral slopes in the visible range are lower than previously reported and exhibit a clear gradient between the Atlantic Ocean and the Mediterranean Sea. Variations reflect the nature of dissolved organic matter, sources and transformation processes.

Phytoplankton absorption is primarily driven by phytoplankton community composition and cell size through the packaging effect and, which in turn affects light absorption efficiency. In the Baltic sea, it is possible to observe filamentous cyanobacteria (Olofsson et al., 2020) which leads to deviations from model predictions such as the B95 model developed by Bricaud et al. (1995). This highlights the limitations of globally derived relationships in specific regional contexts.

For NAP, this study introduces an offset term into the parameterization that was not considered by Babin et al.(2003b). Consistent with previous studies, NAP exhibits a non-negligible absorption in the NIR. Introduction of this offset impacts spectral slope values, resulting in lower spectral slope values than those reported in previous studies. Results highlight the role of chemical composition and aggregation processes such as flocculation (Stramski et al., 2007).

This study demonstrates that, in coastal waters, the regional optical variability cannot be modeled by global water parameterizations and needs its own parameterization taking into account regional specificities (Doxaran et al., 2026). These new regional parameterizations provide improvements for the validation and the calibration of hyperspectral satellite data such as PACE-OCI.

As part of the broader scientific exploitation of the HyperBOOST dataset, the present work will be complemented by forthcoming studies addressing apparent and inherent optical properties, light backscattering, satellite matchups, and additional biogeochemical and bio-optical variables. Together, these studies will provide a comprehensive characterization of European coastal optical environments and support the development of improved coastal bio-optical models and hyperspectral ocean color algorithms.

https://doi.org/10.5194/egusphere-2026-4579
Preprint. Discussion started: 7 September 2026

Authors contribution

Conceptualization, D.D.; methodology, D.D.; Investigation, I.M., C.S, P.P, and D.D.; Data curation: M.C, E.B, and D.D; writing—original draft preparation, P.P.; writing—review and editing, P.P., D.D., C.S, E.B., V.B and V.M.V.; Visualization, P.P; project administration and funding acquisition, V.M.V and D.D. All authors have read and agreed to the published version of the manuscript.

Competing interests

None declared.

Acknowledgements

We gratefully acknowledge Peer Bork for his vision in initiating and shaping the Traversing European Coastlines project. His leadership, invaluable guidance, and intellectual contributions were foundational for this pan-European project. His commitment to advancing collaborative and interdisciplinary research was instrumental to the work reported in this manuscript. Peer passed away before the publication of this manuscript; we honor his memory with profound gratitude and dedicate this work to his enduring scientific legacy.

We thank the Traversing European Coastlines (TREC) Consortium, the TREC core partners EMBL (TREC European Network), the Tara Ocean Foundation (TOF), the Tara Europa Consortium and the European Marine Biological Resource Centre (EMBRC) for their commitment to making the TREC expedition possible.

Special thanks to the TREC Field Work Tara Team, the Tara Ocean Foundation team, the R/V Tara crew, the local TREC partner institutions, and the TREC Expedition Volunteers. Thanks to the scientists and crew of the Tara Europa expedition for their efforts in the collection of quality water samples and to the Tara technical crew and scientists on board for installation of the instrument and management of logistics. We are thankful to the countries for their support in granting sampling permissions.

This publication was enabled by the support of EMBL member states to the TREC expedition, within the framework of EMBL's Molecules to Ecosystems Programme (2022–2026).

This research was supported by research grants from Horizon Europe (through the EU BioOcean5D and Blueremediomics projects) and the European Space Agency (through the HyperBOOST project). This work has been carried out within the framework of the ESA-funded Hyperspectral Bio-Optical Observations Sailing on Tara (HyperBOOST) project (grant number 4000135756/21/I-EF). Emmanuel Boss was also supported by NASA (grant 80NSSC24K0374). We also thank EUMETSAT and the Copernicus Marine Environment and Monitoring Service (CMEMS) for providing free oceancolor satellite data and the European Marine Observation and Data Network (EMODnet) for bathymetry data as these were used to support the sampling design.

https://doi.org/10.5194/egusphere-2026-4579
Preprint. Discussion started: 7 September 2026

We gratefully thank agnès b. and Etienne Bourgois, AXA, Bic, BNP Paribas, Capgemini, L'OREAL, Biotherm, the Veolia Foundation, Neuize OBC, CNR, Bell & Ross, the Groupe EDF Foundation, De Rothschild Foundation, France Collectivités, and our many individual donors who contributed to the success of this endeavor. We also thank our institutional partners: Fonds Français pour l'Environnement Mondial, UNESCO, Office Français de la Biodiversité (OFB), Région Bretagne, Lorient Agglomération, Lyon Metropole, and Terre Bleue Cotentin for their trust and support. This paper is publication number TBD of the Traversing European Coastlines (TREC) expedition.

Financial supports

This research was supported by Horizon Europe through the BioOcean5D and BlueRemediomics projects, and by the European Space Agency (ESA) through the Hyperspectral Bio-Optical Observations Sailing on Tara (HyperBOOST) project (grant no. 4000135756/21/I-EF). Emmanuel Boss was supported by NASA (grant no. 80NSSC24K0374)

Code and data availability

The in situ biogeochemical and optical data collected during the Tara Europa and HyperBOOST campaigns are available at Zenodo via https://doi.org/10.5281/zenodo.19738690. The third-party COASTlOOC dataset used for validation is available at https://doi.org/10.17882/93570.

https://doi.org/10.5194/egusphere-2026-4579
Preprint. Discussion started: 7 September 2026

References

Atwood, E. C., Jackson, T., Laurenson, A., Jönsson, B. F., Spyrakos, E., Jiang, D., Sent, G., Selmes, N., Simis, S., Danne, O., Tyler, A., and Groom, S.: Framework for Regional to Global Extension of Optical Water Types for Remote Sensing of Optically Complex Transitional Water Bodies, Remote Sensing, 16, 3267, https://doi.org/10.3390/rs16173267, 2024.

Babin, M. and Stramski, D.: Variations in the mass-specific absorption coefficient of mineral particles suspended in water, Limnology & Oceanography, 49, 756–767, https://doi.org/10.4319/lo.2004.49.3.0756, 2004.

Babin, M., Morel, A., Fournier-Sicre, V., Fell, F., and Stramski, D.: Light scattering properties of marine particles in coastal and open ocean waters as related to the particle mass concentration, Limnology & Oceanography, 48, 843–859, https://doi.org/10.4319/lo.2003.48.2.0843, 2003a.

Babin, M., Stramski, D., Ferrari, G. M., Claustre, H., Bricaud, A., Obolensky, G., and Hoepffner, N.: Variations in the light absorption coefficients of phytoplankton, nonalgal particles, and dissolved organic matter in coastal waters around Europe, J. Geophys. Res., 108, 2001JC000882, https://doi.org/10.1029/2001JC000882, 2003b.

Bégorre, C., Dabrin, A., Masson, M., Mourier, B., Eyrolle, F., Lepage, H., Morereau, A., and Coquery, M.: Reconstruction of historical suspended particulate matter contributions of Rhône River tributaries to the Mediterranean Sea, Geomorphology, 417, 108445, https://doi.org/10.1016/j.geomorph.2022.108445, 2022.

Bengil, F., McKee, D., Beşiktepe, S. T., Sanjuan Calzado, V., and Trees, C.: A bio-optical model for integration into ecosystem models for the Ligurian Sea, Progress in Oceanography, 149, 1–15, https://doi.org/10.1016/j.pocean.2016.10.007, 2016.

Blasco, T., Migon, C., Morin, G., Dufour, A., Vigier, N., Marty, S., and Doxaran, D.: Carbon stable isotope ratio as a revealer of incomplete decarbonation for particulate organic carbon measurement in river plumes, Geo-Mar Lett, 41, 4, https://doi.org/10.1007/s00367-020-00676-2, 2021.

Bowers, D. G. and Binding, C. E.: The optical properties of mineral suspended particles: A review and synthesis, Estuarine, Coastal and Shelf Science, 67, 219–230, https://doi.org/10.1016/j.ecss.2005.11.010, 2006.

Bowers, D. G., Harker, G. E. L., and Stephan, B.: Absorption spectra of inorganic particles in the Irish Sea and their relevance to remote sensing of chlorophyll, International Journal of Remote Sensing, 17, 2449–2460, https://doi.org/10.1080/01431169608948782, 1996.

Bowers, D. G., Harker, G. E. L., Smith, P. S. D., and Tett, P.: Optical Properties of a Region of Freshwater Influence (The Clyde Sea), Estuarine, Coastal and Shelf Science, 50, 717–726, https://doi.org/10.1006/ecss.1999.0600, 2000.

Bracher, A., Bouman, H. A., Brewin, R. J. W., Bricaud, A., Brotas, V., Ciotti, A. M., Clementson, L., Devred, E., Di Cicco, A., Dutkiewicz, S., Hardman-Mountford, N. J., Hickman, A. E., Hieronymi, M., Hirata, T., Losa, S. N., Mouw, C. B., Organelli, E., Raitsos, D. E., Uitz, J., Vogt, M., and Wolanin, A.: Obtaining Phytoplankton Diversity from Ocean Color: A Scientific Roadmap for Future Development, Front. Mar. Sci., 4, https://doi.org/10.3389/fmars.2017.00055, 2017.

Brando, V., Santoleri, R., Colella, S., Volpe, G., Di Cicco, A., Sammartino, M., González Vilas, L., Lapucci, C., Böhm, E., Zoffoli, M., Cesarini, C., Forneris, V., La Padula, F., Mangin, A., Jutard, Q., Bretagnon, M., Bryère, P., Demaria, J., Calton, B., Netting, J., Sathyendranath, S., D'Alimonte, D., Kajiyama, T., Van Der Zande, D., Vanhellemont, Q., Stelzer, K., Böttcher, M., and Lebreton, C.: Overview of Operational Global and Regional Ocean Colour Essential Ocean Variables Within the Copernicus Marine Service, Remote Sensing, 16, 4588, https://doi.org/10.3390/rs16234588, 2024.

https://doi.org/10.5194/egusphere-2026-4579
Preprint. Discussion started: 7 September 2026

Brewin, R. J. W., Sathyendranath, S., Hirata, T., Lavender, S. J., Barciela, R. M., and Hardman-Mountford, N. J.: A three-component model of phytoplankton size class for the Atlantic Ocean, Ecological Modelling, 221, 1472–1483, https://doi.org/10.1016/j.ecolmodel.2010.02.014, 2010.

Bricaud, A., Babin, M., Morel, A., and Claustre, H.: Variability in the chlorophyll-specific absorption coefficients of natural phytoplankton: Analysis and parameterization, J. Geophys. Res., 100, 13321–13332, https://doi.org/10.1029/95JC00463, 1995.

Bricaud, A., Claustre, H., Ras, J., and Oubelkheir, K.: Natural variability of phytoplanktonic absorption in oceanic waters: Influence of the size structure of algal populations, J. Geophys. Res., 109, 2004JC002419, https://doi.org/10.1029/2004JC002419, 2004.

Chase, A. P., Kramer, S. J., Haëntjens, N., Boss, E. S., Karp-Boss, L., Edmondson, M., and Graff, J. R.: Evaluation of diagnostic pigments to estimate phytoplankton size classes, Limnology & Ocean Methods, 18, 570–584, https://doi.org/10.1002/lom3.10385, 2020.

Costanzo, M., Brando, V., Marchese, C., Jordan, T., and Martinez Vicente, V.: Hyperspectral Bio-Optical Observations Sailing on Tara (HyperBOOST) Collocated In situ Dataset, https://doi.org/10.5281/zenodo.19738690, 2026.

Costanzo, M., Brando, V., Falcini, F., Marchese, C., González Vilas, L., Boss, E., Doxaran, D., Potin, P., Simis, S., Wood, T., Jordan, John, Santinelli, C., bachi, G., Checcucci, G., Tropea, C., Carloni, M., Guerrazzi, M., Valsecchi, S., Evangelista, V., Rio, M.-H., Concha, J. A., De Vargas, C., and Martinez-Vicente, V.: The Hyperspectral Bio-Optical Observations Sailing on Tara (HyperBOOST) dataset. Submitted to Earth System Science Data., n.d.

van Dijk, M. A., Gregori, G., Hoogveld, H. L., Rijkeboer, M., Denis, M., Malkassian, A., and Gons, H. J.: Optimizing the setup of a flow cytometric cell sorter for efficient quantitative sorting of long filamentous cyanobacteria, Cytometry Part A, 77A, 911–924, https://doi.org/10.1002/cyto.a.20946, 2010.

Doerffer, R. and Schiller, H.: The MERIS Case 2 water algorithm, International Journal of Remote Sensing, 28, 517–535, https://doi.org/10.1080/01431160600821127, 2007.

Dogliotti, A. I., Ruddick, K. G., Nechad, B., Doxaran, D., and Knaeps, E.: A single algorithm to retrieve turbidity from remotely-sensed data in all coastal and estuarine waters, Remote Sensing of Environment, 156, 157–168, https://doi.org/10.1016/j.rse.2014.09.020, 2015.

Donlon, C., Berruti, B., Buongiorno, A., Ferreira, M.-H., Féménias, P., Frerick, J., Goryl, P., Klein, U., Laur, H., Mavrocordatos, C., Nieke, J., Rebhan, H., Seitz, B., Stroede, J., and Sciarra, R.: The Global Monitoring for Environment and Security (GMES) Sentinel-3 mission, Remote Sensing of Environment, 120, 37–57, https://doi.org/10.1016/j.rse.2011.07.024, 2012.

Doxaran, D., Ehn, J., Bélanger, S., Matsuoka, A., Hooker, S., and Babin, M.: Optical characterisation of suspended particles in the Mackenzie River plume (Canadian Arctic Ocean) and implications for ocean colour remote sensing, Biogeosciences, 9, 3213–3229, https://doi.org/10.5194/bg-9-3213-2012, 2012.

Doxaran, D., Mayot, I., De Keukelaere, L., Moelans, R., Verdoodt, N., and Knaeps, E.: Understanding the Optical Behavior and Spectral Signature of Dredging-Induced Plumes in Coastal Waters, Remote Sensing, 18, 1428, https://doi.org/10.3390/rs18091428, 2026.

https://doi.org/10.5194/egusphere-2026-4579
Preprint. Discussion started: 7 September 2026

Estapa, M. L., Boss, E., Mayer, L. M., and Roesler, C. S.: Role of iron and organic carbon in mass-specific light absorption by particulate matter from Louisiana coastal waters, Limnology & Oceanography, 57, 97–112, https://doi.org/10.4319/lo.2012.57.1.0097, 2012.

Feist, B. E. and Levin, P. S.: Novel Indicators of Anthropogenic Influence on Marine and Coastal Ecosystems, Front. Mar. Sci., 3, https://doi.org/10.3389/fmars.2016.00113, 2016.

Gattuso, J.-P., Frankignoulle, M., and Wollast, R.: CARBON AND CARBONATE METABOLISM IN COASTAL AQUATIC ECOSYSTEMS, Annu. Rev. Ecol. Syst., 29, 405–434, https://doi.org/10.1146/annurev.ecolsys.29.1.405, 1998.

Guanter, L., Kaufmann, H., Segl, K., Foerster, S., Rogass, C., Chabrillat, S., Kuester, T., Hollstein, A., Rossner, G., Chlebek, C., Straif, C., Fischer, S., Schrader, S., Storch, T., Heiden, U., Mueller, A., Bachmann, M., Mühle, H., Müller, R., Habermeyer, M., Ohndorf, A., Hill, J., Buddenbaum, H., Hostert, P., Van Der Linden, S., Leitão, P., Rabe, A., Doerffer, R., Krasemann, H., Xi, H., Mauser, W., Hank, T., Locherer, M., Rast, M., Staenz, K., and Sang, B.: The EnMAP Spaceborne Imaging Spectroscopy Mission for Earth Observation, Remote Sensing, 7, 8830–8857, https://doi.org/10.3390/rs70708830, 2015.

Hansell, D. A.: Dissolved Organic Carbon Reference Material Program, Eos, Transactions American Geophysical Union, 86, 318–318, https://doi.org/10.1029/2005EO350003, 2005.

Helms, J. R., Stubbins, A., Ritchie, J. D., Minor, E. C., Kieber, D. J., and Mopper, K.: Absorption spectral slopes and slope ratios as indicators of molecular weight, source, and photobleaching of chromophoric dissolved organic matter, Limnology and Oceanography, 53, 955–969, https://doi.org/10.4319/lo.2008.53.3.0955, 2008.

IOCCG Protocol Series (2018). Inherent Optical Property Measurements and Protocols: Absorption Coefficient, Neeley, A. R. and Mannino, A. (eds.), IOCCG Ocean Optics and Biogeochemistry Protocols for Satellite Ocean Colour Sensor Validation, Volume 1.0, IOCCG, Dartmouth, NS, Canada.

IOCCG Protocol Series (2021).Particulate Organic Matter Sampling and Measurement Protocols: Consensus Towards Future Ocean Color Missions. Chaves,J.E., Cetinić,I., Dall'Olmo,G.,Estapa,M., Gardner, W.,Goñi, M.,Graff, J.R.,Hernes, P.,Lam,P.J., Liu,Z., Lomas, M.W., Mannino, M., Novak, M.G., Turnewitsch, R., Werdell, P.J., Westberry, T.K., IOCCG Ocean Optics and Biogeochemistry Protocols for Satellite Ocean Colour Sensor Validation,Volume6.0, IOCCG, Dartmouth, NS, Canada. http://dx.doi.org/10.25607/OBP1646

Keller, D. P., Lenton, A., Littleton, E. W., Oschlies, A., Scott, V., and Vaughan, N. E.: The Effects of Carbon Dioxide Removal on the Carbon Cycle, Curr Clim Change Rep, 4, 250–265, https://doi.org/10.1007/s40641-018-0104-3, 2018.

Loizzo, R., Guarini, R., Longo, F., Scopa, T., Formaro, R., Facchinetti, C., and Varacalli, G.: Prisma: The Italian Hyperspectral Mission, IEEE International Geoscience and Remote Sensing, 175–178, https://doi.org/https://doi.org/10.1109/IGARSS.2018.8518512, 2018.

Marchese, C., Boss, E., Falcini, F., Doxaran, D., De Vargas, C., Pfister, G., and Brando, V.: Satellite Data Sharing for Scientific Inter-Group Cooperation Using the Leaflet R Package, Oceanog, 37, https://doi.org/10.5670/oceanog.2024.513, 2024.

Massicotte, P., Babin, M., Fell, F., Fournier-Sicre, V., and Doxaran, D.: The Coastal Surveillance Through Observation of Ocean Color (COASTℓOOC) dataset, Earth Syst. Sci. Data, 15, 3529–3545, https://doi.org/10.5194/essd-15-3529-2023, 2023.

https://doi.org/10.5194/egusphere-2026-4579
Preprint. Discussion started: 7 September 2026

Matsuoka, A., Boss, E., Babin, M., Karp-Boss, L., Hafez, M., Chekalyuk, A., Proctor, C. W., Werdell, P. J., and Bricaud, A.: Pan-Arctic optical characteristics of colored dissolved organic matter: Tracing dissolved organic carbon in changing Arctic waters using satellite ocean color data, Remote Sensing of Environment, 200, 89–101, https://doi.org/10.1016/j.rse.2017.08.009, 2017.

Muller-Karger, F. E., Varela, R., Thunell, R., Luerssen, R., Hu, C., and Walsh, J. J.: The importance of continental margins in the global carbon cycle, Geophysical Research Letters, 32, https://doi.org/10.1029/2004GL021346, 2005.

Muller-Karger, F. E., Hestir, E., Ade, C., Turpie, K., Roberts, D. A., Siegel, D., Miller, R. J., Humm, D., Izenberg, N., Keller, M., Morgan, F., Frouin, R., Dekker, A. G., Gardner, R., Goodman, J., Schaeffer, B., Franz, B. A., Pahlevan, N., Mannino, A. G., Concha, J. A., Ackleson, S. G., Cavanaugh, K. C., Romanou, A., Tzortziou, M., Boss, E. S., Pavlick, R., Freeman, A., Rousseaux, C. S., Dunne, J., Long, M. C., Klein, E., McKinley, G. A., Goes, J., Letelier, R., Kavanaugh, M., Roffer, M., Bracher, A., Arrigo, K. R., Dierssen, H., Zhang, X., Davis, F. W., Best, B., Guralnick, R., Moisan, J., Sosik, H. M., Kudela, R., Mouw, C. B., Barnard, A. H., Palacios, S., Roesler, C., Drakou, E. G., Appeltans, W., and Jetz, W.: Satellite sensor requirements for monitoring essential biodiversity variables of coastal ecosystems, Ecological Applications, 28, 749–760, https://doi.org/10.1002/eap.1682, 2018.

Neukermans, G., Ruddick, K., Loisel, H., and Roose, P.: Optimization and quality control of suspended particulate matter concentration measurement using turbidity measurements, Limnology & Ocean Methods, 10, 1011–1023, https://doi.org/10.4319/lom.2012.10.1011, 2012.

Olofsson, M., Suikkanen, S., Kobos, J., Wasmund, N., and Karlson, B.: Basin-specific changes in filamentous cyanobacteria community composition across four decades in the Baltic Sea, Harmful Algae, 91, 101685, https://doi.org/10.1016/j.hal.2019.101685, 2020.

Organelli, E., Nuccio, C., Lazzara, L., Uitz, J., Bricaud, A., and Massi, L.: On the discrimination of multiple phytoplankton groups from light absorption spectra of assemblages with mixed taxonomic composition and variable light conditions, Appl. Opt., AO, 56, 3952–3968, https://doi.org/10.1364/AO.56.003952, 2017.

Para, J., Coble, P. G., Charrière, B., Tedetti, M., Fontana, C., and Sempéré, R.: Fluorescence and absorption properties of chromophoric dissolved organic matter (CDOM) in coastal surface waters of the northwestern Mediterranean Sea, influence of the Rhône River, Biogeosciences, 7, 4083–4103, https://doi.org/10.5194/bg-7-4083-2010, 2010.

Pérez, G. L., Galí, M., Royer, S.-J., Gerea, M., Ortega-Retuerta, E., Gasol, J. M., Marrasé, C., and Simó, R.: Variability of phytoplankton light absorption in stratified waters of the NW Mediterranean Sea: The interplay between pigment composition and the packaging effect, Deep Sea Research Part I: Oceanographic Research Papers, 169, 103460, https://doi.org/10.1016/j.dsr.2020.103460, 2021.

Pitarch, J. and Brando, V. E.: A hyperspectral and multi-angular synthetic dataset for algorithm development in waters of varying trophic levels and optical complexity, Earth System Science Data, 17, 435–460, https://doi.org/10.5194/essd-17-435-2025, 2025.

Prieur, L. and Sathyendranath, S.: An optical classification of coastal and oceanic waters based on the specific spectral absorption curves of phytoplankton pigments, dissolved organic matter, and other particulate materials, Limnology and Oceanography, 26, 671–689, https://doi.org/10.4319/lo.1981.26.4.0671, 1981.

Ras, J., Claustre, H., and Uitz, J.: Spatial variability of phytoplankton pigment distributions in the Subtropical South Pacific Ocean: comparison between in situ and predicted data, Biogeosciences, 5, 353–369, https://doi.org/10.5194/bg-5-353-2008, 2008.

https://doi.org/10.5194/egusphere-2026-4579
Preprint. Discussion started: 7 September 2026

Rast, M., Bezy, J. L., and Bruzzi, S.: The ESA Medium Resolution Imaging Spectrometer MERIS a review of the instrument and its mission, International Journal of Remote Sensing, 20, 1681–1702, https://doi.org/10.1080/014311699212416, 1999.

Regnier, P., Friedlingstein, P., Ciais, P., Mackenzie, F. T., Gruber, N., Janssens, I. A., Laruelle, G. G., Lauerwald, R., Luyssaert, S., Andersson, A. J., Arndt, S., Arnosti, C., Borges, A. V., Dale, A. W., Gallego-Sala, A., Goddéris, Y., Goossens, N., Hartmann, J., Heinze, C., Ilyina, T., Joos, F., LaRowe, D. E., Leifeld, J., Meysman, F. J. R., Munhoven, G., Raymond, P. A., Spahni, R., Suntharalingam, P., and Thullner, M.: Anthropogenic perturbation of the carbon fluxes from land to ocean, Nature Geosci, 6, 597–607, https://doi.org/10.1038/ngeo1830, 2013.

Röttgers, R. and Gehnke, S.: Measurement of light absorption by aquatic particles: improvement of the quantitative filter technique by use of an integrating sphere approach, Appl. Opt., AO, 51, 1336–1351, https://doi.org/10.1364/AO.51.001336, 2012.

Röttgers, R., Dupouy, C., Taylor, B. B., Bracher, A., and Woźniak, S. B.: Mass-specific light absorption coefficients of natural aquatic particles in the near-infrared spectral region, Limnology & Oceanography, 59, 1449–1460, https://doi.org/10.4319/lo.2014.59.5.1449, 2014.

Sale, P. F., Agardy, T., Ainsworth, C. H., Feist, B. E., Bell, J. D., Christie, P., Hoegh-Guldberg, O., Mumby, P. J., Feary, D. A., Saunders, M. I., Daw, T. M., Foale, S. J., Levin, P. S., Lindeman, K. C., Lorenzen, K., Pomeroy, R. S., Allison, E. H., Bradbury, R. H., Corrin, J., Edwards, A. J., Obura, D. O., Sadovy de Mitcheson, Y. J., Samoilys, M. A., and Sheppard, C. R. C.: Transforming management of tropical coastal seas to cope with challenges of the 21st century, Marine Pollution Bulletin, 85, 8–23, https://doi.org/10.1016/j.marpolbul.2014.06.005, 2014.

Santinelli, C., Follett, C., Retelletti Brogi, S., Xu, L., and Repeta, D.: Carbon isotope measurements reveal unexpected cycling of dissolved organic matter in the deep Mediterranean Sea, Marine Chemistry, 177, 267–277, https://doi.org/10.1016/j.marchem.2015.06.018, 2015.

Spyrakos, E., O'Donnell, R., Hunter, P. D., Miller, C., Scott, M., Simis, S. G. H., Neil, C., Barbosa, C. C. F., Binding, C. E., Bradt, S., Bresciani, M., Dall'Olmo, G., Giardino, C., Gitelson, A. A., Kutser, T., Li, L., Matsushita, B., Martinez-Vicente, V., Matthews, M. W., Ogashawara, I., Ruiz-Verdú, A., Schalles, J. F., Tebbs, E., Zhang, Y., and Tyler, A. N.: Optical types of inland and coastal waters, Limnology and Oceanography, 63, 846–870, https://doi.org/10.1002/lno.10674, 2018.

Stal, L. J., Albertano, P., Bergman, B., Bröckel, K. von, Gallon, J. R., Hayes, P. K., Sivonen, K., and Walsby, A. E.: BASIC: Baltic Sea cyanobacteria. An investigation of the structure and dynamics of water blooms of cyanobacteria in the Baltic Sea—responses to a changing environment, Continental Shelf Research, 23, 1695–1714, https://doi.org/10.1016/j.csr.2003.06.001, 2003.

Stramski, D., Babin, M., and Woźniak, S. B.: Variations in the optical properties of terrigenous mineral-rich particulate matter suspended in seawater, Limnology & Oceanography, 52, 2418–2433, https://doi.org/10.4319/lo.2007.52.6.2418, 2007.

Tassan, S. and Ferrari, G. M.: An alternative approach to absorption measurements of aquatic particles retained on filters, Limnology and Oceanography, 40, 1358–1368, https://doi.org/10.4319/lo.1995.40.8.1358, 1995.

Tassan, S. and Ferrari, G. M.: Variability of light absorption by aquatic particles in the near-infrared spectral region, Appl. Opt., AO, 42, 4802–4810, https://doi.org/10.1364/AO.42.004802, 2003.

Tran, T. K., Duforêt-Gaurier, L., Vantrepotte, V., Jorge, D. S. F., Mériaux, X., Cauvin, A., d'Andon, O. F., and Loisel, H.: Deriving Particulate Organic Carbon in Coastal Waters from Remote Sensing: Inter-Comparison Exercise and Development of a Maximum Band-Ratio Approach, Remote Sensing, 11, https://doi.org/10.3390/rs11232849, 2019.

https://doi.org/10.5194/egusphere-2026-4579
Preprint. Discussion started: 7 September 2026

Uitz, J., Claustre, H., Morel, A., and Hooker, S. B.: Vertical distribution of phytoplankton communities in open ocean: An assessment based on surface chlorophyll, J. Geophys. Res., 111, 2005JC003207, https://doi.org/10.1029/2005JC003207, 2006.

Van Heukelem, L. and Thomas, C. S.: Computer-assisted high-performance liquid chromatography method development with applications to the isolation and analysis of phytoplankton pigments, Journal of Chromatography A, 910, 31–49, https://doi.org/10.1016/S0378-4347(00)00603-4, 2001.

Vidussi, F., Claustre, H., Manca, B. B., Luchetta, A., and Marty, J.: Phytoplankton pigment distribution in relation to upper thermocline circulation in the eastern Mediterranean Sea during winter, J. Geophys. Res., 106, 19939–19956, https://doi.org/10.1029/1999JC000308, 2001.

Ward, N. D., Bianchi, T. S., Medeiros, P. M., Seidel, M., Richey, J. E., Keil, R. G., and Sawakuchi, H. O.: Where Carbon Goes When Water Flows: Carbon Cycling across the Aquatic Continuum, Front. Mar. Sci., 4, https://doi.org/10.3389/fmars.2017.00007, 2017.

Werdell, P. J., Cairns, B., Caplan, S. A., Cetinić, I., Foley, S. R., Franz, B. A., Gao, M., Fasnacht, Z. T., Huemmrich, K. F., Ibrahim, A., Knobelspiesse, K. D., Mannino, A., McKinna, L. I. W., Poulin, C., Rajapakshe, C., and Sayer, A. M.: Advancing Earth System Science With the NASA Plankton, Aerosol, Cloud, Ocean Ecosystem (PACE) Satellite Mission, Global Change Biology, 32, e70869, https://doi.org/10.1111/gcb.70869, 2026.

Woźniak, S., Litwicka, D., and Stoń-Egiert, J.: Variability and relationships between the size, composition and optical properties of suspended particulate matter in the coastal waters of western Spitsbergen, assessed through measurements of size-fractionated seawater samples, OCEANOLOGIA, 66, https://doi.org/10.5697/EZNP4044, 2024.

Zibordi, G. and Berthon, J.-F.: Coastal Atmosphere and Sea Time Series (CoASTS) and Bio-Optical mapping of Marine Properties (BiOMaP): the CoASTS-BiOMaP dataset, Earth System Science Data, 16, 5477–5502, https://doi.org/10.5194/essd-16-5477-2024, 2024.